STRUCTURE & DYNAMICS OF BLOCK COPOLYMER MICELLES IN THE PRESENCE OF COSOLVENTS

A Thesis

Presented to

the Faculty of the Department of Chemical and Biomolecular Engineering

University of Houston

In Partial Fulfillment

of the Requirements for the Degree

Master of Science

in Chemical Engineering

by

Avantika Singh

December 2013

STRUCTURE & DYNAMICS OF BLOCK COPOLYMER MICELLES IN THE PRESENCE OF COSOLVENTS

Avantika Singh

Approved:

Chair of the Committee
Megan L. Robertson, Assistant Professor
Chemical and Biomolecular Engineering

Committee Members:

Jeffrey D. Rimer, Assistant Professor
Chemical and Biomolecular Engineering

Haleh Ardebili, Assistant Professor
Mechanical Engineering

Suresh K. Khator, Associate Dean,
Cullen College of Engineering

Michael P. Harold, Professor and Chair
Chemical and Biomolecular Engineering

ACKNOWLEDGEMENTS

I would like to express my gratitude to my thesis advisor, Dr. Megan L. Robertson, for her continuous mentoring throughout this research work, which has been essential for bringing this thesis to reality. She has been an inspiration in a lot of ways and has exemplified striving and working hard, which drove me to give my best.

I would also like to extend my gratitude to Dr. Jeffrey D. Rimer and Dr. Haleh Ardebili for serving on my thesis committee. On the experimental side, there are many people who have helped with the micelle characterization as well as the neutron scattering experiments. Special mention goes to Dr. Peter G. Vekilov and Dr. Jeffrey D. Rimer for allowing us to use their DLS instruments. The cumulant code used in the micellar size analysis was provided by Dr. Rimer's research group. At the neutron scattering facilities, Dr. Paul Butler at NIST has been very kind with his insightful suggestions on performing the experiment and Dr. Lilin He at ORNL for his assistance with the experiments. On the data fitting side, the Matlab code used in this work to fit the form factor would not have been possible without the help of my two great colleagues and friends, Kedar Grama and Mike Byington. Their expertise with the programming made a lot of analysis possible in a very short period of time, for which I am very grateful. I would also like to thank Dr. Katerina Kourentzi and Dr, Richard Wilson's group for their valuable suggestions for the fluorescence side of this project.

I am highly indebted to my wonderful and supportive lab members, Brian Rohde, Shu Wang, Vivek Yadav and Guozhen Yang who have helped me in

many big and small ways. Sharing stories, success and failures with them has made it a very worthwhile experience. A very important part of my time here has also been mentoring and working alongside with the undergraduate students, Maria Marquez, Ashish Bhattarai and Michelle Xie, from whom I have learned a great deal and I am very thankful for their contribution to this project.

I would like to thank all of my friends whose continuous support has always the best part to cherish, especially my roommates Anupam Aich and Balakrishnan Ramesh, who have become my family here. Finally and most importantly, I am grateful to my beloved parents and kiddo sister, who have always believed in me, and have been there to support and encourage me at all times.

STRUCTURE & DYNAMICS OF BLOCK COPOLYMER MICELLES IN THE PRESENCE OF COSOLVENTS

An Abstract

of

Thesis

Presented to

the Faculty of the Department of Chemical and Biomolecular Engineering

University of Houston

In Partial Fulfillment

of the Requirements for the Degree

Master of Science

in Chemical Engineering

by

Avantika Singh

December 2013

ABSTRACT

Amphiphilic diblock copolymers, which form micelle structures in selective solvents, offer a great advantage of tunability in physical characteristics as compared to low molecular weight surfactants. Block copolymer micelles in aqueous solvents are a subject of great interest in drug delivery applications for their high loading capacity and targeted drug delivery. We aim to understand the kinetic and thermodynamic processes which underlie the self-assembly of diblock copolymer micelle systems. The present work focuses on diblock copolymers containing blocks of poly(ethylene oxide) (a hydrophilic polymer) and polycaprolactone (a hydrophobic polymer), which spontaneously self-assemble into spherical micelles in water. Addition of a common good solvent (co-solvent) for both of the constituting blocks, such as tetrahydrofuran (THF), reduces the interfacial tension at the core-corona interface. We are currently investigating the effect of this phenomenon on the micelle structural properties and their dynamics, using the neutron scattering experiments. Structural parameters of interest include hydrodynamic radius, core radius, corona thickness, aggregation number, and the degree of swelling of the micelle core with the co-solvent. In addition, dynamic property of interest is the characteristic time scale of single chain exchange (unimers) between the micelles. Both structural and dynamic parameters are examined as the interfacial tension at the core-corona interface is varied through changing the co-solvent concentration.

TABLE OF CONTENTS

LIST OF FIGURES

LIST OF TABLES

CHAPTER 1

INTRODUCTION

Surfactants are amphiphilic molecules which spontaneously self-assemble when dissolved in a selective solvent, resulting in different micellar morphologies, and sizes varying from the nm to μm range[1]. The realization that surfactants can be used to mimic biological structures like cell membranes, enzymes and liposomes has generated considerable interest in exploration of these materials[2]. Presently the domain of surfactant applications has extended far beyond biological mimics in engineering detergents, enzymes, emulsions, catalysis, and as potential drug delivery vehicles.

Diblock copolymers are a class of such amphiphilic molecules, composed of two distinct polymer chains (i.e., blocks) joined together by a covalent bond (Figure 1.1a). Polymeric micelles have many advantages over conventional low molecular weight surfactants as they have more robust and tunable structures, low critical micelle concentrations (CMCs), and higher loading capacity. Additionally, their exchange kinetics occur over more relevant time scales which can be tuned over a wide range (milliseconds-hours)[1, 3].

Controlling the molecular characteristics of the two blocks in the diblock copolymer provides a method of designing amphiphilic molecules with specific properties. Factors that affect the self-assembly can be broadly divided in two categories: polymer-related properties and solvent conditions. Polymer-related properties are a result of the chosen polymer synthesis parameters including the molecular weight of the copolymer, ratio of the two blocks, chemical

composition, and the polymer architecture. Solvent conditions include the selected solvent or the co-solvent mixtures, temperature, pH, and the presence of additives (ions and surfactants)[4]. The resulting self-assembled structures can assume different morphologies, for example, spherical micelles (Figure 1.1b), cylindrical micelles, or vesicles, depending on these parameters[3].

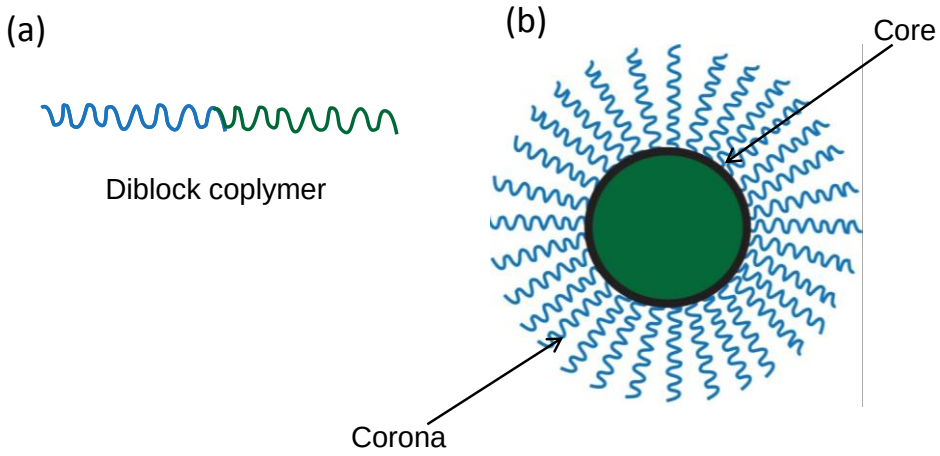

Figure 1.1. (a) Illustration of an amphililic diblock copolymer & (b) Illustration of a spherical micelle structure.

The driving force behind the micellization process is the minimization of the micelle free energy. Three main contributions to this free energy are: free energy of the core, chain stretching of the corona and free energy of the core-corona interface[4c, 5]. Several studies have focused on determining the conditions and parameters that control the self-assembly of polymeric micelles. Both tuning factors, polymer-related and solvent conditions, effect one or more of these three terms. Of these factors, changing the solvent condition is a facile way of altering the interfacial energy, and hence tuning the system for a given set of polymer characteristics and architecture[6].

1.1. Modifying micelle dimensions and structure by tuning interfacial tension

Tuning the solvent quality, and therefore the interfacial tension, is a convenient method to manipulate the micelle structure and size. This idea has been employed in work by Einsenberg and co-workers, who demonstrated the reversible transition in size of poly(styrene-*b*-acrylic acid) (PS-PA) vesicles in dioxane/water and dioxane/tetrahydrofuran (THF)/water mixtures[4a]. Changing the ratio of dioxane to THF, and changing the water content controlled the vesicle size. Increasing the THF content in THF/dioxane mixtures led to smaller sizes in vesicles. Adding water to dioxane-rich solutions led to an increase in size, but no significant effect was found of water addition to THF rich solutions. Therefore, they were successful in creating a vesicle system that is sensitive to changes in water content. Additives such as NaOH, HCl or NaCl, also worked to effect the electrostatic repulsions among the corona of PA chains, and hence, a change in aggregation properties.

In a study by Lund and co-workers, they investigated the role of addition of dimethylformamide (DMF) as a co-solvent in poly(ethylene-*co*-propylene-*b*-ethylene oxide) (PEP-PEO) block copolymer micelles[7]. Their main findings were the reduction in aggregation number of these micelles with increasing content of DMF, along with reduction in the micelle size. Also, no significant change was found in the radius of gyration (R_g) of pure PEO chains alone in pure water and in water/DMF mixtures, indicating that the R_g for PEO chains was not considerably affected if the corona block selective solvent is added.

Continuing to address the importance of role of interfacial tension on micelle core-corona interface, work by Epps group, showed how the micelle core size and corona thickness could be controlled with co-solvent (THF) addition[6c]. By minimizing the scattering contributions from corona, they elucidated the change in core-corona interfacial thickness with co-solvent addition. High THF content led to a broader core-corona interface. Another important conclusion was the presence of swollen micelle cores, such that the co-solvent composition in the core was higher than the bulk composition.

Lund et al. studied the structural transition from spherical to cylindrical micelles by altering the solvent quality using co-solvent mixtures[8]. They applied an elaborate thermodynamic model as a function of interfacial tension to understand the details of structures as well as their morphological transition. Altering the interfacial tension had significant effect on both the core and corona chain stretching.

A number of theoretical[9] and experimental[6c,d,10] works have been completed in the last two decades to understand the properties which arise from the micelle structure. Small-angle neutron scattering has emerged as a powerful technique for characterizing the micelle structure, where the method of contrast variation can selectively highlight different components of the micellar structure. For instance, replacing either the core or the corona block with an equivalent deuterated polymer and varying the contrast of the solvent to match the corona, can effectively emphasize the detailed structure of the core.

Lodge and co-workers examined the micellar core and corona profiles separately by selectively match the scattering length density (SLD) of solvent to either the core or corona for the poly(styrene-*b*-isoprene) (PS-PI) micelles[6d]. They were able to extract important information on micellar structures such as core radius, overall size, aggregation number, solvent fraction in the core and corona thickness, with respect to changes in temperature. Pedersen and coworkers selectively deuterated the polymer dPS-PI to compare the experimental data with scattering functions derived from Monte Carlo simulations, and found good agreement[11]. Their results indicated the presence of solvent in the core which was slowly exchanging with the bulk solvent.

1.2. Manipulating dynamics in block copolymer micelles by tuning interfacial tension

Dynamic equilibrium is also known to exist in surfactant solutions, which makes the study of kinetics of surfactants imperative for understanding the self-assembly processes. Although the chain exchange kinetics for small molecule surfactants is well understood[12,13] pathways to equilibrium are not very well understood[14]. In contrast, polymeric nanostructures are often arrested in metastable states because of high activation barriers and extremely slow kinetics, and may sometimes never be able to reach their global free energy minimum[8,15]. Additionally certain conditions such as crystallinity, entanglements and vitrification of the core block can cause block copolymer micelles to exhibit much slower time scales[16]. Kinetic pathways in such frozen micelles determine the structural properties such as the aggregation number, micelle size and their

stability[16a, 17,18]. This is important information to ensure reproducible micelle preparation and prediction of long term performance.

This fact has been utilized successfully by Eisenberg and co-workers[4b, 5, 19] and Cui et al.[19] to design complicated structures via kinetic control of assembly processes. Despite the recent advancement in the synthesis of these fascinating structures, a detailed understanding of the kinetics is essential not only to validate true equilibrium, but the information on pathways traversed can also help design polymeric structures for a plethora of applications such as targeted drug delivery[20], organic photovoltaics[21], viscosity modification[16c] and colloidal and polymer blend stabilization[22].

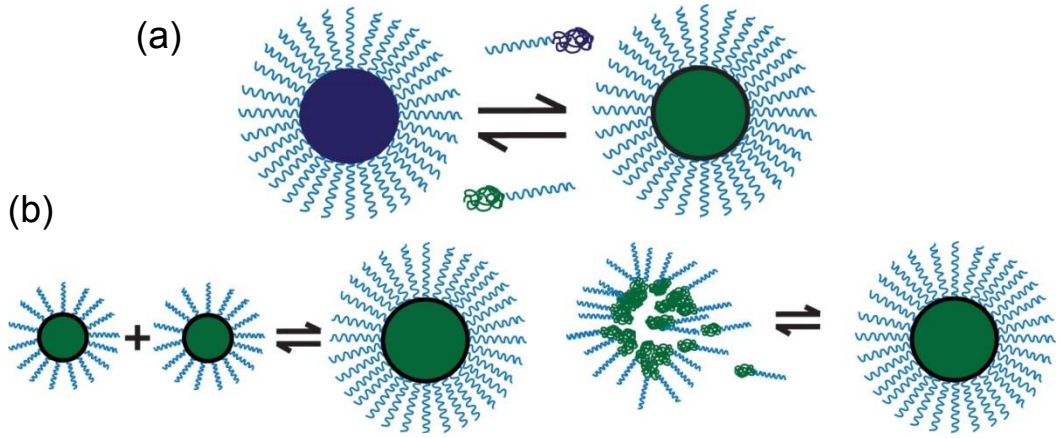

Figure 1.2. (a) Cartoon of single chain insertion-expulsion mechanism and (b) Cartoon of micelle fusion/fission mechanisms.

Regarding the micelle formation process, there are competing theories in literature predicting different association mechanism for micelle growth. In direct analogy with the Aniansson-Wall mechanism[12, 23], developed for low molecular weight compounds, single chain exchange is predicted for polymeric micelles when perturbed close to equilibrium (Figure 1.2a)[24]. For perturbations

far from equilibrium there are two competing theories. Single chain insertion/expulsion is suggested by Nyrkov and Semenov[15,25], while Dormindotiva illustrated how fission/fusion mechanisms may be more relevant (Figure 1.2b)[26].

The traditionally employed strategy used either fluorescence quench spectroscopy[27] or the temperature jump experiments[28] to probe micelle dynamics. These experimental techniques caused significant perturbations from equilibrium, due to the presence of bulky fluorescent groups or high temperature jumps, therefore the distribution in relaxation rates was not very well understood.

Lund et al. investigated the micellization process by using *in situ* small angle X-ray scattering which provided millisecond temporal resolution[29]. Initially, PEP-PEO chains were dissolved in pure DMF where only single chains (unimers) exist, and then self-assembly was triggered by addition of water resulting in a jump in interfacial tension. Since water and DMF have different interfacial tensions with the core block, changing the solvent quality provides a very useful means of analyzing the evolution of micellar morphology.

Won et al. studied spherical and cylindrical micelles of poly(butadiene-b-polyethylene oxide) (PB-PEO) copolymers in water and found no chain exchange over a period of 8 days[16a]. They concluded that systems which have a high degree of segregation (high number of repeat units in both the hydrophilic and hydrophobic blocks) with overall low hydrophilicity are trapped in their initial aggregate structures. Building on this, Lund and co-workers

investigated PEP-PEO block copolymer micelles in DMF/water with shorter hydrophobic length and longer hydrophilic length of the polymers using novel time resolved- small angle neutron scattering (TR-SANS) exchange technique, which enables study of chain exchange in an equilibrium state[3, 18].

Their main findings emphasized the role of interfacial tension in molecule exchange kinetics. Under high surface tension conditions between the core block and the solvent, such as in water, chain kinetics were frozen and no chain exchange was detected. However, upon reducing the interfacial tension by addition of a good co-solvent, DMF in this case, some chain exchange was detected. An intriguing observation from their study was the logarithmic decay of the relaxation curves. Unlike small molecule surfactants which are marked by a single exponential decay with a time constants of the order of ms-μs, polymer micelles are characterized by a logarithmic decay of relaxation times with time constants ranging from minutes to days. From the theory by Halperin and Alexander, a single rate constant is expected based on the energy activation barrier for a chain to expulse from the hydrophobic core molecule exchange, analogous to the mechanism in low molecular weight surfactants[25]. This broad distribution in relaxation could not be attributed to the relatively narrow polydispersity in the core block. Therefore it was proposed to be a combined effect of chain coupling during the expulsion process imposed by the geometric constraints of polymeric micelles. This question was further investigated by the Bates and co-workers for PS-PEP micelles in organic solvent with a more symmetric block compositions[30]. They successfully explained the logarithmic

distribution in decay rates to be a consequence of the hypersensitivity of the chain kinetics on the core block length distribution, or polydispersity of the core block, as opposed to hypothesis by Lund et al.[3, 31].

1.3. Objective

The prospect of applications in drug delivery has drawn considerable interest towards amphiphilic copolymers containing biodegradable and biocompatible components which have high loading capacity and can be modified to include targeting groups. The model system chosen for this project is a diblock copolymer of poly(ethylene oxide-*b*-ε-caprolactone) (PEO-PCL), and the solvent selected is water, as it is prevalent in all biological systems. Poly(ethylene oxide) (PEO) is hydrophilic and forms the corona, while polycaprolactone (PCL) is hydrophobic and forms the core. PEO-PCL is an attractive choice for targeted drug delivery as the polymers are biocompatible and partially biodegradable[32].

Hypothesis 1: The micelle structural parameters will be highly dependent on the nature of the solvent-core and solvent-corona interactions. Tuning solvent quality through addition of a co-solvent will be an effective method of manipulating and deeply understanding micelle structural parameters.

Hypothesis 2: The presence of the solvent additive will greatly influence the polymer chain and micelle dynamics. Tuning the solvent quality through the addition of a co-solvent will be an effective method of manipulating the dynamic processes in these systems.

We aim to understand the kinetic and thermodynamic processes which underlie the self-assembly and exchange dynamics of diblock copolymer micelle systems. Addition of a common good solvent (co-solvent) for both of the constituting blocks, such as tetrahydrofuran (THF), reduces the interfacial tension at the core-corona interface. We are currently investigating the effect of this phenomenon on the micelle structural properties and their dynamics, using scattering experiments. Structural parameters of interest include hydrodynamic radius, core radius, corona thickness, aggregation number, core-corona interfacial width, degree of swelling of the micelle core with the co-solvent, and unimer (free chain) concentration. In addition, dynamic properties of interest are the characteristic time scale of unimer exchange between micelles, micelle diffusion coefficients, and the molecular dynamics of individual (core and corona) blocks. We are examining these structural and dynamic parameters as the interfacial tension at the core-corona interface is varied through changing the co-solvent concentration. Fundamental knowledge from these studies will inform design of drug delivery systems by allowing us to tailor micelle properties for optimal drug loading as well as targeted and timed uptake.

CHAPTER 2

MATERIALS and METHODS

2.1. Synthesis and characterization of diblock copolymers

All chemicals were purchased from Sigma Aldrich unless otherwise specified. ε-Caprolactone (>97%) was purified by distillation over calcium hydride (CaH_2). The catalyst 1,5,7-Triazabicyclo[4.4.0]dec-5-ene (TBD), was used as received and stored in the glove box to prevent its deactivation. Poly(ethylene oxide-*b*-ε-caprolactone) (PEO-PCL) diblock copolymers were synthesized using monomethoxy-PEO (purchased from Polymer Source, M_n = 2 and 5 kg/mol) as a macroinitiator for the ring-opening polymerization of ε-CL (Figure 2.1). ε-caprolactone (ε-CL) was added to a solution of predissolved TBD and PEO initiator in benzene, following a detailed procedure described in the literature[33]. The benzene (ACS reagent, min 99%) used as the polymerization solvent was distilled twice over CaH_2 to remove any contaminants prior to use. The reaction was quenched by the addition of benzoic acid (>=99.5%). A similar procedure was followed for polymerization of deuterated caprolactone (d_6) (purchased from CDN Isotopes, Canada, 98% atom D), resulting in PEO-dPCL block copolymers, with the only difference being that the deuterated monomer was used as received. The polymers were dissolved in tetrahydrofuran (THF) (chromatography grade, >=99.5%, inhibitor free) for precipitation in hexanes, (ACS grade, >99%) and dried for a day under vacuum at room temperature. They were then heated to 60°C for another 8

hours in the vacuum oven. NMR was performed on final dried samples to ensure that no residual solvent peaks were evident.

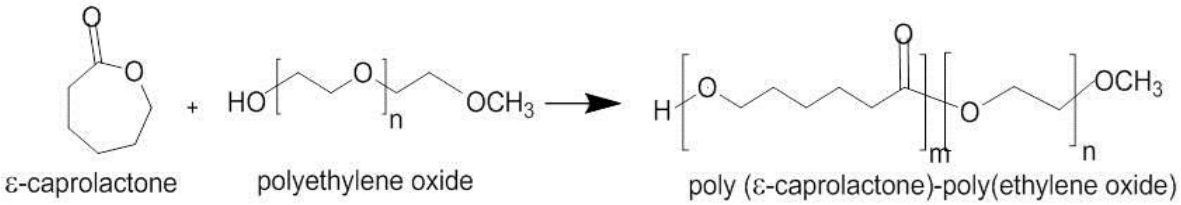

Figure 2.1. Schematic of diblock copolymer synthesis to form poly(ethylene oxide)-*b*-poly(caprolactone).

Proton nuclear magnetic resonance (^{1}H-NMR) was performed on JEOL 500 Hz spectrometer and characteristic peaks of PEO, PCL and ε–CL monomer were identified at 3.64 ppm, 4.05 ppm and 4.22 ppm, respectively. The relative peak areas were used to determine the percent conversion of ε–CL into polymer, as well as the weight fractions of the PEO and PCL blocks, and the number-average molecular weight (M_n). The synthesized polymers are denoted by PEO_X-PCL_Y, where X and Y represent the number-average molecular weight of the individual blocks. The dried polymers were analyzed with a Malvern Viscotek gel permeation chromatography (GPC) instrument for obtaining polydispersity index (PDI). THF (chromatography grade, >=99.9%) was used as the mobile phase at 30 °C and the column was calibrated using 12 narrow polystyrene standards. The final characteristics for the copolymers used in this study are given in the Table below (Table 2.1).

Table 2.1. Polymer Characteristics[a].

Polymer Sample	M_n PEO-PCL (kg/mol)	N_{PEO}	N_{PCL}	W_{PCL}	PDI
Structure Study					
PEO_{2k}-$hPCL_{3k}$	5	44	27	0.59	1.09
PEO_{5k}-$hPCL_{8k}$	12.5	113	66	0.59	1.17

Table 2.1. (continued)					
Dynamics Study					
Experiment 1					
E polymers					
PEO_{2k}-$dPCL_{4k}$	5.6	44	33	0.65	1.71
PEO_{2k}-$hPCL_{4k}$	5.4	44	31	0.62	1.64
Experiment 2					
A polymers					
PEO_{2k}-$dPCL_{2k}$	3.8	44	16	0.50	1.08
PEO_{2k}-$hPCL_{2k}$	3.9	44	17	0.48	1.05
B polymers					
PEO_{2k}-$dPCL_{3k}$	4.8	44	25	0.60	1.09
PEO_{2k}-$hPCL_{3k}$	4.6	44	26	0.58	1.04
Experiment 3					
B polymers (same as before)					
PEO_{2k}-$dPCL_{3k}$	4.8	44	25	0.60	1.09
PEO_{2k}-$hPCL_{3k}$	4.6	44	26	0.58	1.04
C polymers					
PEO_{5k}-$dPCL_{5k}$	10.1	113	45	0.51	1.14
PEO_{5k}-$hPCL_{5k}$	10.3	113	47	0.51	1.15

[a]M_n= Number-average molecular weight (by NMR), N_{PEO} and N_{PCL}= number of repeat units in PEO and PCL, respectively (by NMR), W_{PCL}= weight fraction of PCL in the block copolymer (by NMR), PDI= polydispersity index of block copolymer (by GPC using conventional calibration), h and d refers to hydrogenated or deuterated PCL.

2.2. Micelle preparation by solvent switch method

All chemicals were purchased from Sigma Aldrich unless otherwise specified. Inhibitor-free tetrahydrofuran (THF) (EMD Millipore, >=99.5%, H_2O <=0.02%) was used as purified from a solvent purification column (Pure Process Technology). Inhibitor-free deuterated tetrahydrofuran (THF-d_8, high purity NMR solvent, 99.5% atom D) and heavy water (D_2O, 99.9% atom D)

were used without any purification. Water (H_2O) was purified using a Millipore MilliQ Gradient water purification system (containing RO cartridge, UV lamp).

20 mg of block copolymer was dissolved in the required amount of THF and subsequently water (H_2O or D_2O) was very slowly added through a syringe pump, at a rate of 0.2 mL per minute, as described in the literature[34]. The micelle solutions were sonicated (VWR Symphony, 35 kHz) at room temperature for an hour and then filtered using a 0.2 µm Nylon syringe filter (purchased from VWR) prior to being transferred to glass cuvettes for dynamic light scattering (DLS) measurements.

2.3. Dynamic light scattering (DLS)

An ALV light scattering instrument with a goniometer and ALV-5000/EPP multiple tau digital correlator was employed to conduct DLS experiments with a He-Ne laser of wavelength 632.8 nm. The detector angle was 90 degrees and the measurements were made at 25 °C. The raw autocorrelation data looked unimodal for every sample (Figure 2.2).

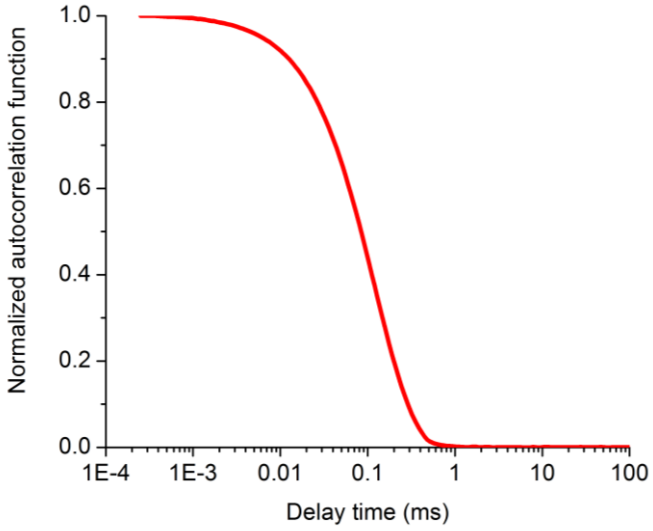

Figure 2.2. Unimodal DLS correlation curve for PEO_{2k}-PCL_{3k} micelle solution prepared in 20% THF/80% D_2O

The normalized correlation function generated from the ALV correlator was fit using an in-house built Matlab code based on Cumulant Analysis, which is described in chapter 3. The hydrodynamic radius of the diffusing particles was obtained using the Stokes-Einstein relation given by

$$R_h = \frac{k_B T}{6\pi \eta D}, \tag{2.1}$$

where, from $D,\ k_B\ T,\ \eta$ are the diffusion coefficient of the micelle, Boltzman's constant, temperature and viscosity of the solution respectively. The viscosity for water/ THF mixtures at 298K were obtained from literature[35].

2.4. Small angle neutron scattering (SANS) for structural study

2.4.1. SANS experimental set-up

Small angle neutron scattering (SANS) experiments were conducted at the High Flux Isotope Reactor (HFIR) at the CG-2 beamline, Oak Ridge National Laboratory (ORNL), Tennessee. The neutron wavelength was 4.72 Å and two sample to detector distances were used, 1.7m and 18.5m, covering a scattering vector range of 0.0028 to 0.533 $Å^{-1}$. After shipment to HFIR, samples were sonicated for an hour before being exposed to the beam for data collection. Corrections to the data for the empty Hellma cell, background scattering (blocked beam), sample transmission, and detector efficiency were accounted for, using the Spice SANS reduction macro for Igor Pro provided by the scientists at the CG-2 beamline. The absolute intensity was calculated through two methods. For the majority of the data presented in this document, the open beam scattering was used to calibrate the absolute intensity, without the use of standards. Due to an equipment issue during the data collection,

some data sets were calibrated to an absolute scale using an aluminum standard. The two methods were in close agreement (i.e. less than 2% difference between them).

2.4.2. SANS data fitting

A detailed SANS model for data fitting was required to extract information on the characteristics of spherical block copolymer micelles. This model used here was developed by Pedersen and coworkers[10c] and has been employed in other studies [6c,d,10e].

The model contains four contributions: self-correlation of the spherically homogenous core, self-correlation of the Gaussian chains, correlation between the core and the corona, and self-correlation of the corona and is described as

$$F_{mic}(q) = N_{agg}^2\beta_{core}^2A_{core}^2(q) + N_{agg}\beta_{corona}^2P_{Chain}(q) + 2N_{agg}^2\beta_{Core}\beta_{corona}A_{Core}(q)A_{Corona}(q) + N_{agg}(N_{agg}-1)\beta_{corona}^2A_{corona}^2(q). \quad (2.2)$$

In the above equation, N_{agg} is the aggregation number of the micelle (number of diblock copolymer chains in an individual micelle), β_{Core} and β_{corona} are the total excess scattering length densities of the core block and the corona block respectively, which are defined as

$$\beta_{core} = v_{core}(\rho_{core} - \rho_{solvent}) \quad (2.3)$$

and $$\beta_{corona} = v_{corona}(\rho_{corona} - \rho_{solvent}). \quad (2.4)$$

Here, v_{core} and v_{corona} are the volumes of the hydrophobic block and the hydrophilic block respectively. ρ_{core}, ρ_{corona} and $\rho_{solvent}$ are the scattering length densities of the core block, corona block, and the solvent, respectively.

The scattering amplitude of a spherically homogeneous core of radius R with a smooth decay at the surface is defined as

$$A_{core}(q) = \frac{3[\sin(qR) - (qR)\,cos(qR)]}{(qR)^3} \tag{2.5}$$

where the first term is the form factor amplitude of a sphere with a fixed radius R, and the second exponential term accounts for a smooth decay of the scattering length density at the core-corona interface. Here, σ_{int} is the width of the core-corona interface. The chain correlation term for non-interacting Gaussian chains with a radius R_g can be written as

$$P_{Chain}(q) = 2\left[\frac{\exp\left(-q^2R_g^2\right) - 1 + q^2R_g^2}{q^4R_g^4}\right]. \tag{2.6}$$

The corona, composed of mutually non-interacting and self-avoiding chains, can be described by assuming a radial density profile for the extended hydrophilic polymers in two domains of dimension *s* (Figure 2.3.) described as

$$\rho_1 = \frac{4(r-R-s)^3 - (r-R-2s)^3}{4s^3}, \qquad for\ R \le r \le R+s \tag{2.7.1}$$

$$\rho_1 = \frac{-(r-R-2s)^3}{4s^3}, \qquad for\ R+s \le r \le R+2s \tag{2.7.2}$$

$$\rho_1 = 0, \qquad elsewhere \tag{2.7.3}$$

and

$$\rho_2 = \frac{-(r-R-2s)^3}{4s^3}, \qquad for\ R \le r \le R+2s \tag{2.8.1}$$

$$\rho_2 = 0, \qquad elsewhere. \tag{2.8.2}$$

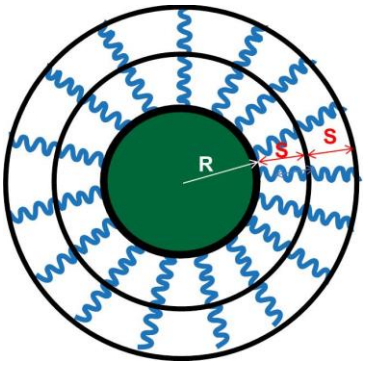

Figure 2.3. Illustration of relative length parameters, core radius, R and width of profile, s.

The total radial density profile of the corona block is written as

$$\rho_{corona}(r) = \frac{\rho_1(r) + a_1\rho_2(r)}{1 + a_1}. \tag{2.9}$$

Here a_1 is the weighing factor for the two profiles.

The Fourier transform this density profile, which is the sum of two cubic b splines, was also analytically calculated by Pedersen and coworkers[10c]

$$A_1 = c_{norm1}^{-1}\left[\begin{array}{c} \frac{24\cos[q(R+2s)]}{q^6} + \frac{6(R+2s)\sin[q(R+2s)]}{q^5} \\ -\frac{96\cos[q(R+s)]}{q^6} \\ +\frac{24(R+s)\sin[q(R+s)]}{q^5} \\ +\frac{4(q^3Rs^3 + 3q^2Rs + 18)\cos[qR]}{q^6} \\ -\frac{2((2q^2s^3 - 9(R-2s)))\sin[qR]}{q^5} \end{array}\right], \tag{2.10}$$

where

$$c_{norm1} = s^4\left(\frac{15R^2 + 14Rs + 5s^2}{5}\right)$$ and

$$A_2 = c_{norm2}^{-1}\left[\begin{array}{l}\dfrac{96\cos[q(R+2s)]}{q^6}+\dfrac{24(R+s)\sin[q(R+s)]}{q^5}\\ +\dfrac{4(q^4Rs^3-6q^2s(R-s)-24)\cos[qR]}{q^6}\\ -\dfrac{4((q^2s^2(3R-s)\ -\ 6(R-3s)))\sin[qR]}{q^5}\end{array}\right], \qquad (2.11)$$

where

$$c_{norm2} = s^4\left(\frac{15R^2+6Rs+s^2}{15}\right).$$

The parameter *s* is related to the width of the profile. The corona can be assumed to consist of two smaller sub-shells of dimension *s*, and the corona density profile in the two parts is given by Equations 2.7-2.11. The two radial densities are linearly combined to yield the overall contribution for the corona self-correlation, where a_1 is the same parameter described above. The exponential term again describes the smoothly decaying scattering length density at the core-corona interface given by

$$A_{corona}(q) = \frac{A_1(q)+a_1A_2(q)}{1+a_1}\exp\left(-\frac{q^2\sigma_{int}^2}{2}\right). \qquad (2.12)$$

The final intensity term includes a Schulz-Zimm distribution for the micelle core radius, described as

$$G(R) = \frac{R^Z}{\Gamma(Z+1)}\left[\frac{Z+1}{R_c}\right]^{Z+1} exp\left[\frac{-(Z+1)R}{R_c}\right], \qquad (2.13)$$

where, $G(R)$ is used to weigh the contributions of scattering intensity originating from micelle radii of different sizes, R_c is the average core size and Z is related to the polydispersity in the core radius, σ_R by

$$\sigma_R^2 = \frac{1}{(Z+1)}. \quad (2.14)$$

The coherent intensity is normalized by the concentration of the micelles (c) and micelle mass (M_{mic}) and then added to the incoherent background, providing the absolute scattering intensity expressed as

$$I(q) = \frac{c}{M_{mic}} \int F_{mic}(q) G(R) dR + bkgd. \quad (2.15)$$

Intermicellar interactions were neglected at the low concentrations employed in this study, therefore no structure factor was included. The six fitting parameters in the above equations are: N_{agg}, $\emptyset_{THF}^{core}$ (the percent of THF in the core which is related to R_c- details described in chapter 3), σ_{int}, s, a_1, σ_R.

2.5. Time resolved- small angle neutron scattering (TR-SANS) for dynamic study

2.5.1. TR-SANS experiment setup

TR-SANS experiments were conducted at the National Institute of Standards and Technology (NIST) on beamline NG-7. A neutron wavelength of 6 Å was employed as well as sample to detector distances of 13m, 4m and 1m, resulting in q-range of 0.0035-0.59 $Å^{-1}$. Corrections to the data for the empty quartz cell, background scattering (blocked beam), sample transmission, and detector efficiency were accounted for, using the SANS reduction macro for Igor Pro provided by the NIST scientists[36]. The open beam scattering was used to calibrate the absolute intensity, without the use of standards.

2.5.2. TR-SANS data fitting

The basis of this technique is the difference in the scattering lengths of hydrogen (h) and deuterium (d). It is a clean method to detect the exchange of chains between micelles at equilibrium. Two sets of polymeric micelles containing either hydrogenated PCL (h-PCL) or deuterated PCL (d-PCL) as the core polymer are prepared separately in a solvent whose scattering length density is matched to the average scattering length density of a 50/50 mixture of d-PCL and h-PCL. The two micelle solutions are mixed together at t=0. As the h and d polymer chains exchange between micelles, the scattering intensity decreases over time. Once the micelle cores contain equal numbers of h-PCL and d-PCL chains, there is no contrast with the solvent background, and the scattering becomes negligible[18,3, 30].

TR-SANS data is analyzed by examining the variation of *I(q)* with respect to time. The chain exchange process can be quantified in time by a relaxation function which is defined as

$$R(t) = \left[\frac{I(t) - I(\infty)}{I(0) - I(\infty)}\right]^{1/2}. \qquad (2.16)$$

Here $I(0)$ corresponds to the average intensity from the h and d cores at time t=0 (before mixing) and $I(\infty)$ is the intensity from a sample containing completely mixed cores (50/50 h-PCL and d-PCL chains) after enough time has elapsed (which is the same as intensity from a premixed h/d sample). Both $I(0)$ and $I(\infty)$ are integrated over the entire *q*-range. $I(t)$ is the excess intensity at any time t, also integrated over the *q*-range.

We are following the concentration flux function to fit our relaxation curve $R(t)$, developed by Choi et al.[30], which accounted for the thermodynamic penalty of extracting chains from the micelle core due to unfavorable core-solvent interactions, as well as the polydispersity of the polymer chains

$$K(t,N) = exp\left[-t\frac{6\pi^2 kT}{N^2 b^2 \zeta}\exp(-\alpha\chi N\right]. \tag{2.17}$$

The polydispersity in the core block is accounted by a Gaussian distribution function expressed as

$$P(N) = \frac{1}{\sigma(N)\sqrt{2\pi}}\exp\left(-\frac{(N-\langle N\rangle)^2}{2\sigma(N)^2}\right), \tag{2.18}$$

and the final relaxation function is given by

$$R(t) = \int_0^\infty P(N)K(t,N)dN. \tag{2.19}$$

CHAPTER 3

MICELLE STRUCTURAL CHARACTERIZATION

3.1. Introduction

The structures of PEO_{2k}-$hPCL_{3k}$ micelles were investigated for an in-depth study of the effect of co-solvent addition through the use of DLS and SANS. The characteristics of the polymers used are listed in Table 2.1. DLS experiments probed the diffusion coefficients and hydrodynamic radii of the micelles. The elaborate model employed for fitting the SANS data reveals fine details about micelle structure such as the core radius, aggregation number, overall micelle size, percent of THF in the core, and other relevant parameters.

The SANS experiments employed contrast variation techniques, in which the hydrogen (h) and deuterium (d) content of the solvent is varied, to elucidate details of the micelle structure and increase the reliability of determining fitting parameters in the model. Micelles were prepared in THF/H_2O mixtures containing 10-50% THF using three different h/d solvent compositions: dTHF/D_2O (C series), 50/50 hTHF/dTHF / 50/50 H_2O/D_2O (E series) and hTHF/D_2O (A series). Through these three solvent compositions, the scattering length density (SLD) of the solvent, and hence the contrast between the core and solvent, and corona and solvent, was varied. The characterization of these three series of micelle solutions by DLS and SANS is described in the following sections.

3.2. Characterization of micelles by DLS

3.2.1 Calculation of diffusion coefficients and hydrodynamic radii

The samples were analyzed through DLS to determine their hydrodynamic radii. The autocorrelation function obtained from the ALV instrument was analyzed using a Matlab code of cumulant analysis. In case of polydisperse systems, the correlation decay, $g_1(q, t_d)$ can be written as a series expansion of all possible decays[37]:

$$\ln\, g_1(q, t_d) = \sum_{n=1}^{\infty} k_n\,(q)\frac{(-\,t_d\,)^n}{n!}$$
$$= -Dq^2\,t_d\, +\, \sigma^2 q^4\,\frac{{t_d}^{\,2}}{2!} + higher\ order\ terms, \qquad (3.1)$$

where k_n is known as the n[th] cumulant. Equation 3.1 shows that the first order cumulant is related to the average diffusion coefficients of the polydisperse particles, while the second order cumulant is related to the standard deviation σ of the distribution of diffusion coefficients. PEO_{2k}-PCL_{3k} micelles were prepared by the solvent switch method at different THF concentrations for the three series and the DLS results are summarized in Tables 3.1-3.3.

Table 3.1. Diffusion coefficients and hydrodynamic radius for C series.

Sample ID	dTHF / D_2O	Diffusion Coefficient ($\times 10^{-11}$ m^2/s)	Hydrodynamic Radius (nm)
C1	10/90	2.43	7.68
C2	20/80	1.99	7.63
C3	30/70	1.67	7.91
C4	40/60	1.45	8.49
C5	50/50	1.41	8.89

Table 3.2. Diffusion coefficients and hydrodynamic radius for E series.

Sample ID	h/dTHF / H_2O/D_2O	Diffusion Coefficient ($\times 10^{-11}$ m^2/s)	Hydrodynamic Radius (nm)
E1	10/90	2.82	6.60
E2	20/80	2.77	5.48
E3	30/70	1.98	6.67
E4	40/60	1.80	6.88
E5	50/50	1.46	8.59

Table 3.3. Diffusion coefficients and hydrodynamic radius for A series.

Sample ID	hTHF / D_2O	Diffusion Coefficient ($\times 10^{-11}$ m^2/s)	Hydrodynamic Radius (nm)
A1	10/90	2.54	7.32
A2	20/80	2.52	6.02
A3	30/70	1.82	7.25
A4	40/60	1.67	7.41
A5	50/50	1.38	9.12

3.2.2. Discussion of viscosities used in DLS analysis

An important consideration in this analysis was the viscosity values for water THF/mixtures. THF/water mixtures are a non-ideal solution, resulting in greater values for the mixture viscosities as compared to either of the pure solvents. Therefore, literature data were used for the solvent mixture viscosities (Figure 3.1), and fitted using a polynomial function through the data, to interpolate at the THF volume fractions of interest[35, 38]. The obtained viscosity values are listed in Table 3.1. An illustrative polynomial equation that was used to fit the data for THF mole fractions $\leq$ 0.15 is shown in the Figure 3.1.

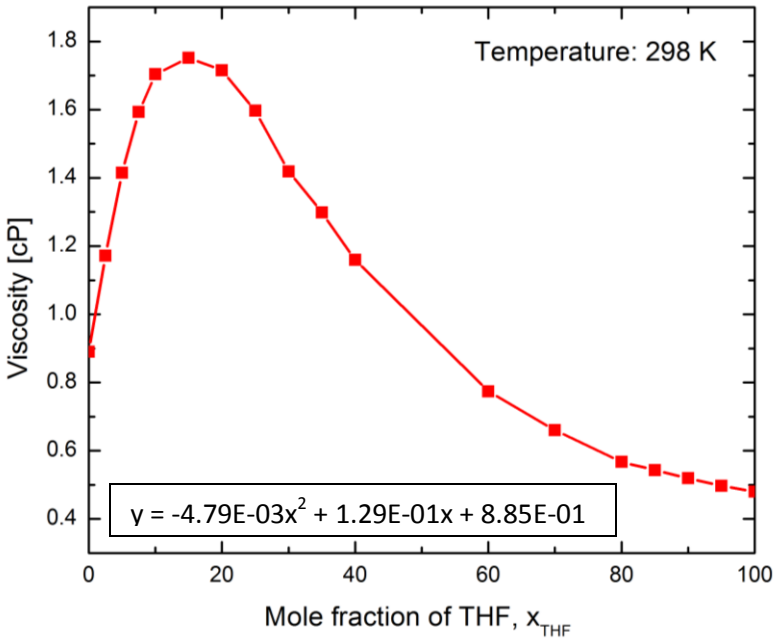

Figure 3.1. Viscosity of THF-H_2O at 298 K[1]

Table 3.4. Viscosity values for THF/H_2O mixtures obtained by interpolating the polynomial fit to the data from ref. 1.

% THF	Viscosity (cP)
10	1.171
20	1.436
30	1.652
40	1.761
50	1.735

From Tables 3.1-3.3, it is evident that the diffusion coefficient decreases as the THF co-solvent fraction is increased. Using the values in Table 3.4 for the solvent viscosities, the hydrodynamic radius was calculated based on Equation 2.1, which correspondingly increases with higher THF content.

We hypothesize the reasoning for this effect could be the micelle core becoming increasingly solvated with the co-solvent, swelling the core. The results of the SANS data fitting will provide additional information on the effect of the THF content on the micelle dimensions.

3.3. Fitting of the micelle form factor model to the SANS data

The model used for data fitting is an elaborate micelle form factor model as described in section 2.4.2, which allows us to determine the detailed features of the micelle structure. This expression has four major contributions arising from the structure of the micelle: self-correlation of the core, self-correlation of the corona, correlation between the core and the corona, and the self- correlations of the Gaussian chains in the corona.

3.3.1. Influence of different fitting parameters on the model fit to the data

Six fitting parameters are included in this model to obtain the final intensity expression, five of which appear in the form factor of the micelle, and the sixth, the polydispersity of the micelle core (σ_R) appears in the Schulz Zimm distribution function. The five fitting parameters which are extracted through the form factor are:N_{agg}, $\emptyset_{THF}^{core}$, σ_{int}, s and a_1. The calculation of other model parameters that aren't employed as fitting parameters is discussed in Section 3.3.2. The volume of THF present in the core and the amount of core-forming polymer in the block copolymer (PCL in our system) present in the core (fixed by N_{agg} and the volume of a PCL-block) comprise the core volume, defining the core radius, R_c. A more detailed discussion on this concept is presented in section 3.3.4. The micelle core radius, R_c, affects three of the micelle form factor terms in its contribution to the overall intensity: the core self-correlation contribution, the corona self-correlation contribution (since the size of the corona shell depends on the core radius), and the core-corona cross-correlation term. Similarly, the width of the core-corona interface (σ_{int}) also

affects the same three contributions which are influenced by the core radius. The parameter s which is related to the width of the corona profile, and the weighing parameter for the two corona amplitude functions a_1, appear in the corona term, and also affect the correlation term between the core and the corona. The presence of many fitting parameters, and intricate relationships between the fitting parameters leads to many challenges in achieving a fit to the data that contains physical meaning. It is possible to find different combinations of the fitting parameters that will each result in little error between the model fit and data. In the proceeding sections, we will describe our approach to fitting the micelle form factor model to the data.

3.3.2. Calculation of constant parameters

The scattering length of the corona was calculated for each of these three series, following Equation 2.4. The volume of a corona block molecule (PEO in our system), $\boldsymbol{v_{corona}}$, was estimated from its molecular weight (M_n PEO = 2 kg/mol) and its mass density of 1.12 g/cm^3. Similarly, the volume of a core block molecule, v_{core} (PCL in our system, M_n = 3 kg/mol, density = 1.14 g/cm^3) was calculated. The total volume of one polymer molecule, $v_{polymer}$,was determined through summing the core and corona block volumes, and multiplying by the block copolymer density, $\rho_{polymer}$, of 1.13 g/cm^3 gave mass of a polymer chain. The samples were prepared at a concentration of 1 wt.%, which was used as a constant in the model. The mass of an individual micelle was determined by the aggregation number and the mass of a diblock copolymer chain as defined in Equation 3.1

$$M_{micelle} = v_{polymer} \times \rho_{polymer} \times N_{agg}. \quad (3.1)$$

3.3.3. Estimation of R_g of PEO chains

The contribution from the self-correlation of the Gaussian PEO chains was held constant by fixing the R_g value to a literature value. Both THF and H_2O are selective solvents for PEO homopolymer. The SANS measurements on PEO chains (M_n = 6 kg/mol) performed by the Epps group[6c] did not indicate any significant change in the R_g value of PEO in varying THF/H_2O ratio mixtures. Averaging over their reported R_g values from 10-50% THF allowed calculation of the statistical segment length of PEO in these solvent mixtures (0.69 nm).[6c] This value of the statistical segment length was used to calculate the R_g value for the PEO used in our study (M_n = 2 kg/mol), and the resulting value was R_g = 1.87 nm. The value of R_g was not fit directly in the SANS profile as the contribution from the self-correlation of corona chains is significantly smaller than the other four terms, and the results of fitting R_g would have little meaning.

3.3.4. Model fitting methods employed in this study

In the analysis presented below, it should be noted that the fits of the model to the data were performed using the micelle form factor model alone as no free chains were detected by pulse field gradient-NMR. This information was provided by our collaborator, Dr. Louis Madsen at Virginia Tech.

In the following discussion we will elucidate the effect of changing different fitting parameters. The approach that we have found to be the most useful is to minimize the sum of the relative errors. One representative fit to the

SANS intensity data (for sample C1) is illustrated in Figure 3.2. This approach provides the best fit across the entire *q*-range, as compared to other possible minimization functions. For example, minimizing the sum of least squares failed as some of the corona parameters were more sensitive in low-q range (where there are high intensities), and resulted in poor fits in the intermediate q-range (where there are low intensities). Use of the relative error avoids this complication. There are still some issues with the confidence in the fitting results since the effect of most of the fitting parameters is prevalent across a large *q*-range (Figure 3.2), and attainment of a unique solution (global minimum) is difficult. A more robust fitting method is currently being investigated. Due to the complicated methods described here, we will focus this discussion on fitting the C and E series data sets individually. Then, we will describe an approach that will be employed in the future to simultaneously fit the C, E and A series, providing much greater confidence in the fitting parameters.

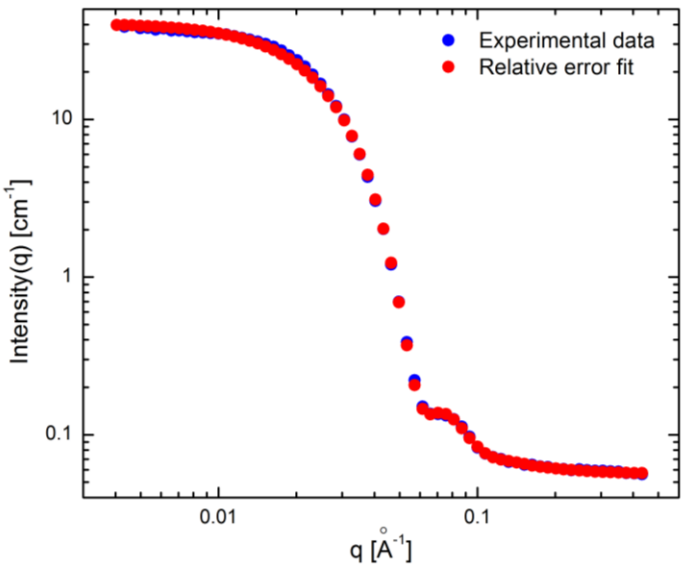

Figure 3.2. Illustrative relative error minimization fit to the SANS intensity data collected for sample C1.

Information from literature indicates the presence of swollen cores due to the co-solvent penetration in the core. However, studies[10c, 10e] that fit this micelle form factor assume a homogeneous spherical core of radius R_c, and the excess scattering length of the core is calculated by taking the difference of the SLD of the core-forming block in the block copolymer and the SLD of the bulk solvent composition. In these studies, the effect of swelling the core with the co-solvent on the SLD of the core was not accounted for. In the analysis presented here, R_c was determined indirectly, by fitting the amount of THF in the core, and assuming the spherical micelle core contains both the core-forming block of the block copolymer and the THF that is present. Therefore, in our fitting methods, R_c was not a fitting parameter, and instead the fraction of THF in the core was the fitting parameter employed. R_c was calculated directly from the fitted value of the % THF in the core as

$$R_c = \left[\frac{3}{4\pi}(v_{core-polymer} + v_{THF-core})\right]^{0.33}, \quad (3.2)$$

where, $v_{core-polymer}$ is the total volume of the core block polymer present in the core and the $v_{THF-core}$ is the volume of THF present in the core.

The SLD of the solvated core was also calculated from the THF content in the core by using the ratio of volume fractions of the THF in the core to the core-forming block of the block copolymer. If x is the volume fraction of the THF in the core, then the SLD of the solvated core ($\rho_{sol-core}$) can be written as

$$\rho_{sol-core} = x\rho_{THF} + (1-x)\rho_{core-block.} \quad (3.3)$$

The excess scattering length of the core (β_{core}) was modified to

$$\beta_{core} = v_{core}\ (\rho_{sol-core} - \rho_{solvent}), \qquad (3.4)$$

where v_{core} is the volume of the swollen core normalized by N_{agg} to account for excess scattering length from one swollen chain. This makes the expression 3.4 still valid for use with the Equations described in section 2.4.2.

3.3.5. Discussion of the effect of the fitting parameters on the model fit

In the following discussion, one fitting parameter is varied while the others are held constant. The purpose of this discussion is to show the effect of each fitting parameter on the intensity profile obtained from the model.

3.3.5a) Effect of % THF in the core: As explained above, increased swelling of the core causes the core radius, R_c, to increase, assuming the aggregation number, N_{agg}, is held constant. In Figure 3.4, we see the effect of the change in core radius (or the related parameter, percent THF in the core) in almost the entire q-range except at very low and very high q values. The core radius also affects the q-value at which the intensity decays.

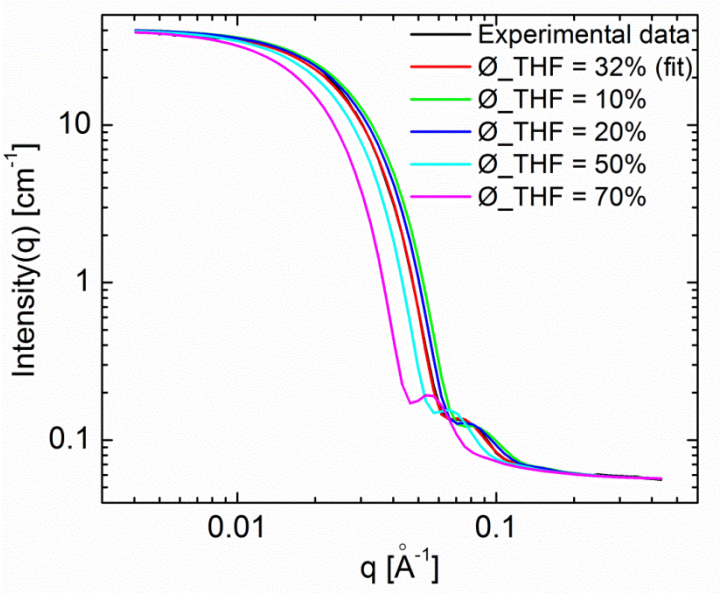

Figure 3.3. Intensity profiles illustrating the effect of the % THF in the core.

3.3.5b) Effect of N_{agg}: The aggregation number scales the entire scattering intensity profile, weighed by the contributions of the four different terms (Figure 3.3). Since at very low q values, all the contributions to the form factor tend to be a constant, changing the value of N_{agg} shifts increases or decreases the low-q intensity.

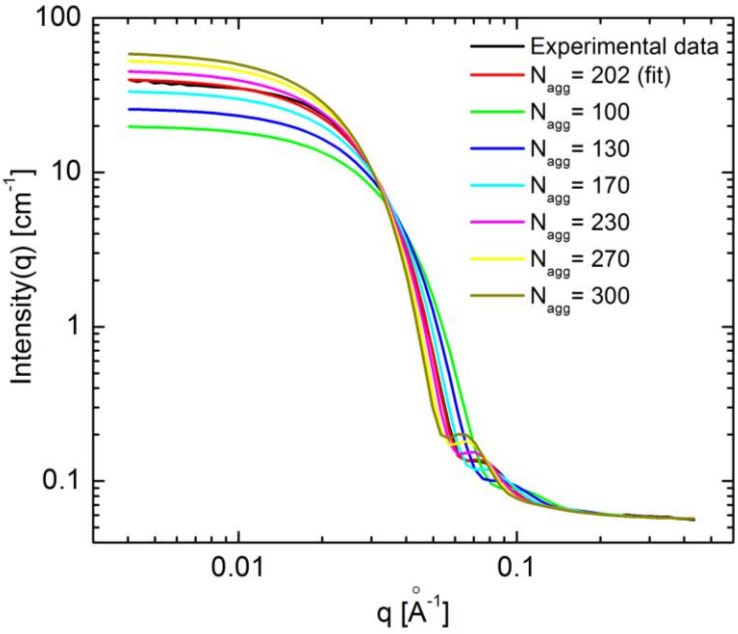

Figure 3.4. Intensity profiles illustrating the effect of the N_{agg} in the core.

3.3.5c) Effect of a_1*:* The corona density profiles is comprised of two contributions, an inner and outer shell containing different polymer density profiles, which are scaled by the parameter a_1. Increasing the value of a_1 implies that a greater contribution is considered from the outer shell (further away from the center of the micelle). The parameter a_1 affects the curvature at low *q* as well as the shape of the corona profile at intermediate *q* (Figure 3.5).

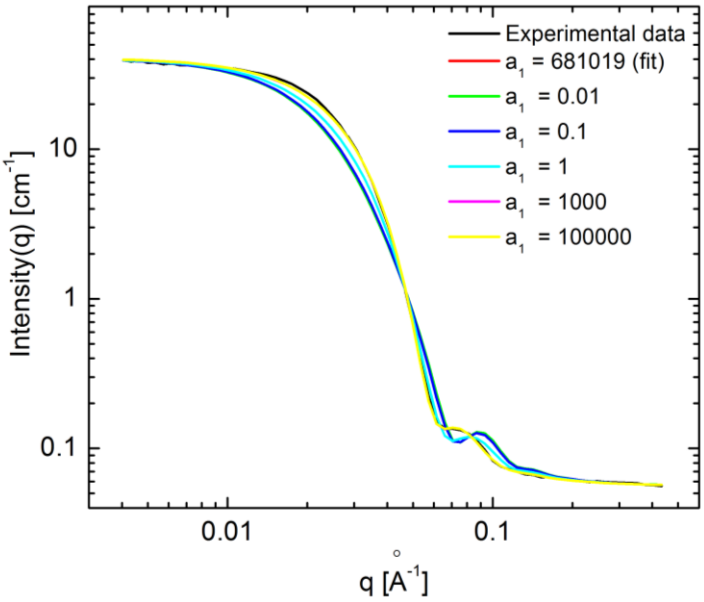

Figure 3.5. Intensity profiles illustrating the effect of parameter a_1 .

3.3.5d) Effect of s: The width of the corona profile is related to the parameter s, such that twice the value of s is the range over which the PEO chain density in the shell extends in the solution, and tends to zero. It affects both the curvature at low *q* and has a significant contribution in determining the shape of the corona profile at intermediate *q* (Figure 3.6).

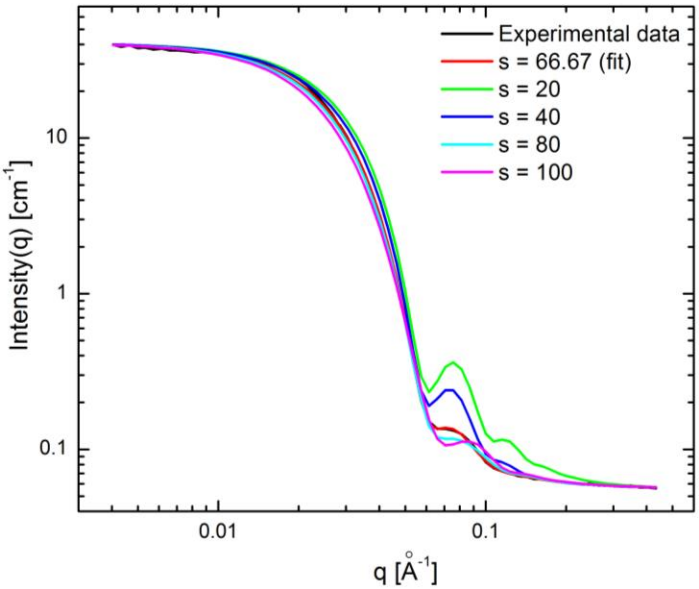

Figure 3.6. Intensity profiles illustrating the effect of the parameter s.

3.3.5e) Effect of σ_{int}: The presence of co-solvent causes the width of the core-corona interface to become more diffuse due to co-solvent swelling the micelle core and is no longer marked by a sharp interface which is observed in highly selective solvent micelle systems. Since it allows for a smooth decay of the form factor amplitude at the core and corona interface, σ_{int} affects the same regions as the micelle core radius, and increasing its value dampens the features present in at intermediate *q* (Figure 3.7).

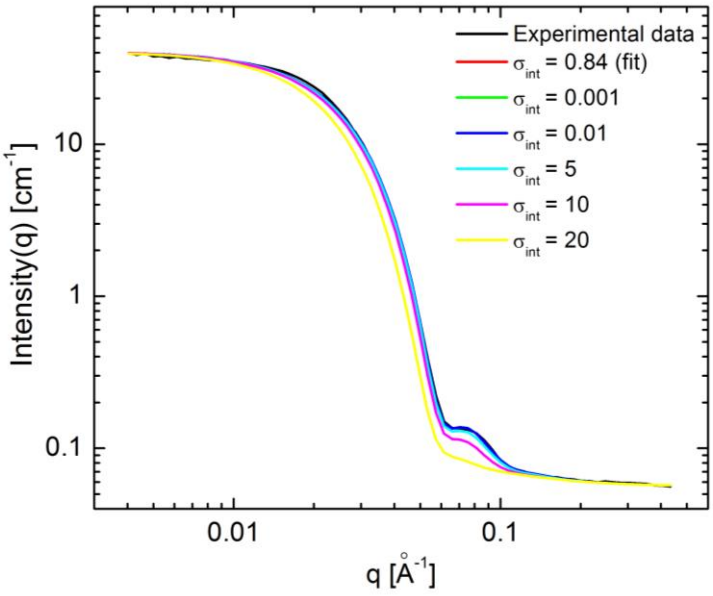

Figure 3.7. Intensity profiles illustrating the effect of the core-corona interfacial width.

3.3.5f) Effect of σ_R: Increasing polydispersity of the core radius affects the features evident at intermediate *q* (Figure 3.8). Higher values of σ_R have the effect of smearing the intensity profile, while the smaller values of σ_R highlighten the features in intermediate *q.*

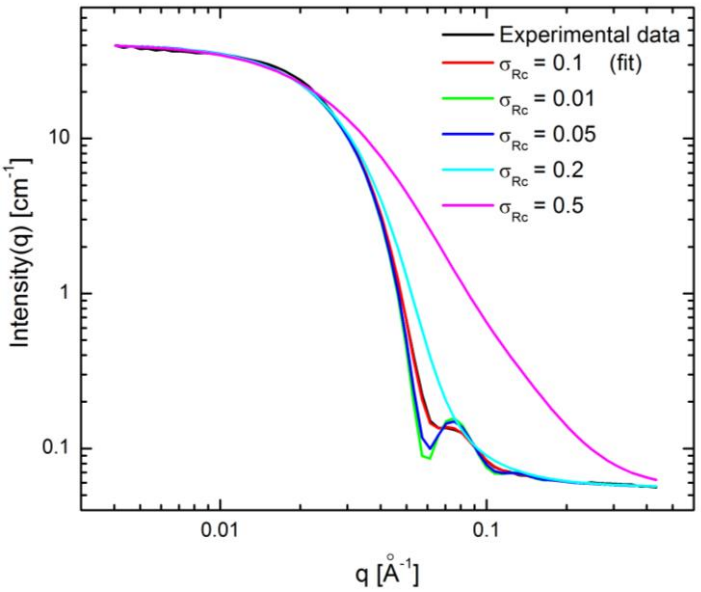

Figure 3.8. Intensity profiles illustrating the effect of the polydispersity in the core radii.

3.4. Results and discussion of fitting the C and E series

The method of contrast variation is a useful technique to identify the effect of co-solvent on micelle structure and its degree of swelling. The SANS intensity profiles were fit using the form factor model, programmed in Matlab, and were compared across different co-solvent mixtures. The fit results from the C series and the E series are summarized in Table 3.5 and Table 3.6 respectively. In the following discussion, we will see the effect of varying the co-solvent concentration on each of the critical micelle structure parameters.

Table 3.5. Fit results from C series, prepared in d-THF/D_2O.

ID	THF [%]	N_{agg}	σ_{int} (Å)	R_m (Å)	a_1	s (A)	σ (R_c)	R_c (Å)	$H=R_m-R_c$ (Å)	%THF core
C1	10	202.89	0.89	108	681019.2	67.86	0.10	65.2	42.76	32.84
C2	20	206.76	5.64	112	80000.00	67.08	0.11	70.5	41.50	45.89
C3	30	190.87	7.00	103	5000.00	42.00	0.12	75.4	27.53	59.37
C4	40	124.39	1.96	105	793807.5	63.45	0.13	70.7	34.30	67.72
C5	50	67.49	0.01	105	2.65	24.67	0.17	68.5	36.47	80.75

Table 3.6. Fit results from E series, prepared in 50/50 h/d-THF / 50/50 H_2O/D_2O.

ID	THF [%]	N_{agg}	σ_{int} (Å)	R_m (Å)	a_1	s (A)	σ (R_c)	R_c (Å)	$H=R_m-R_c$ (Å)	%THF core
E1	10	258.51	2.57	128	11367.53	93.55	0.17	71.3	56.64	34.78
E2	20	210.98	3.37	102	6203.21	44.36	0.11	72.1	29.81	48.60
E3	30	187.91	6.16	113	844.66	71.68	0.16	69.0	43.97	47.58
E4	40	149.85	2.62	97	6212.84	38.79	0.11	71.1	25.88	61.81
E5	50	85.14	1.59	86	12084.58	27.22	0.24	68.3	17.62	75.56

***Effect on aggregation number**:* There is a clear trend in the aggregation number, which decreases with increasing THF content for both the series, consistent with the trend reported in literature[6c, d].

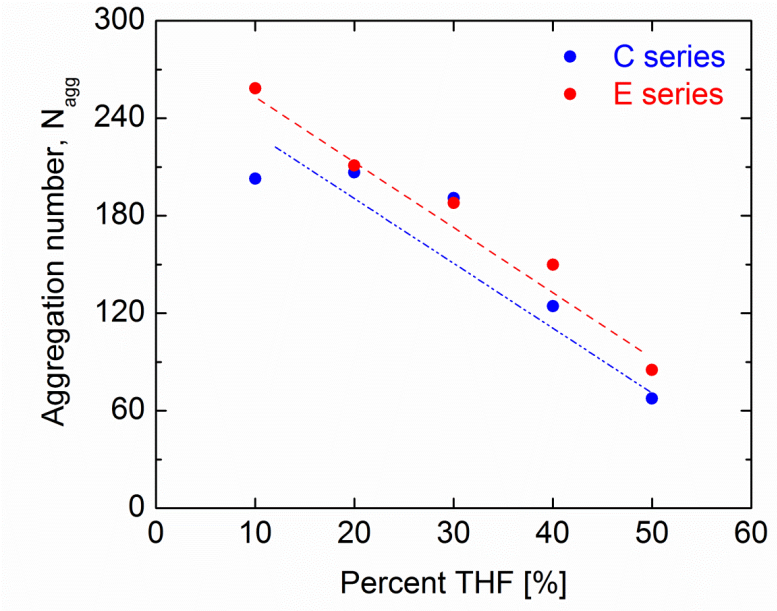

Figure 3.9. Aggregation numbers for C and E series.

Effect on %THF in the core: For both the series, the percent THF in the core increased as the THF concentration in the bulk increased, and it was consistently higher than the percentage present in the bulk solvent. Similar trends were reported by Epps group where they found their PB micelle cores to be significantly swollen[6c].

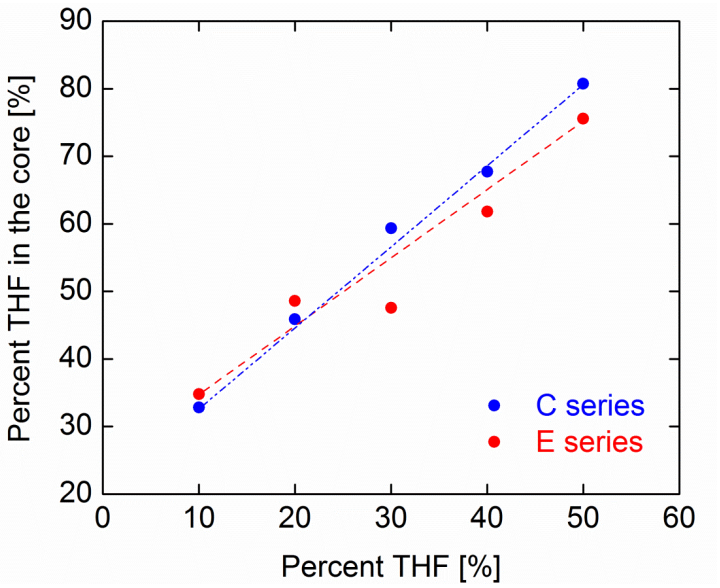

Figure 3.10. Variation of % THF in the core with % THF in C & E series.

Effect on micelle core radius: The micelle core radius changed very little as the THF content was increased: the effect of swelling of the core with THF and the decrease in aggregation number with increasing THF content have opposite effects on the micelle core radius, which appear to almost exactly counteract one another. As that trend is very minimal, it is most likely within the error of determining the R_c values.

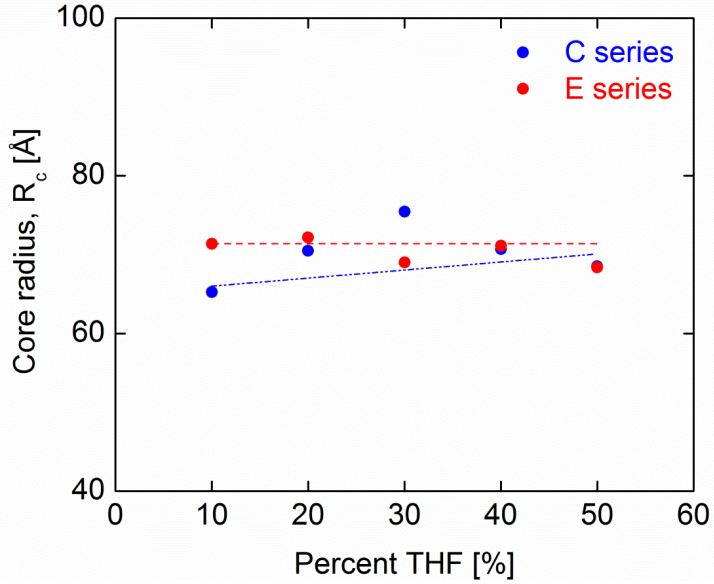

Figure 3.11. Variation of core radius with % THF in C & E series.

Effect on the overall micelle size and the corona thickness: The corona profile was evaluated by calculating a rescaled corona density profile, $\hat{\rho}_{corona}(r)$, using the parameter s obtained from the SANS fitting[6c, d, 10c]. The corona density profile was integrated over the volume of the micelle shell, and rescaled by setting it equal to the total volume of PEO chains present in the corona as

$$\int 4\pi\hat{\rho}_{corona}(r)r^2dr = N_{agg}v_{corona}. \quad (3.5)$$

The plots for the rescaled corona profiles $\hat{\rho}_{corona}(r)$ are presented in Figure 3.11 and 3.12 for C and E series respectively. The starting point for the corona density profiles is the micelle core radius as determined by the fitting results.

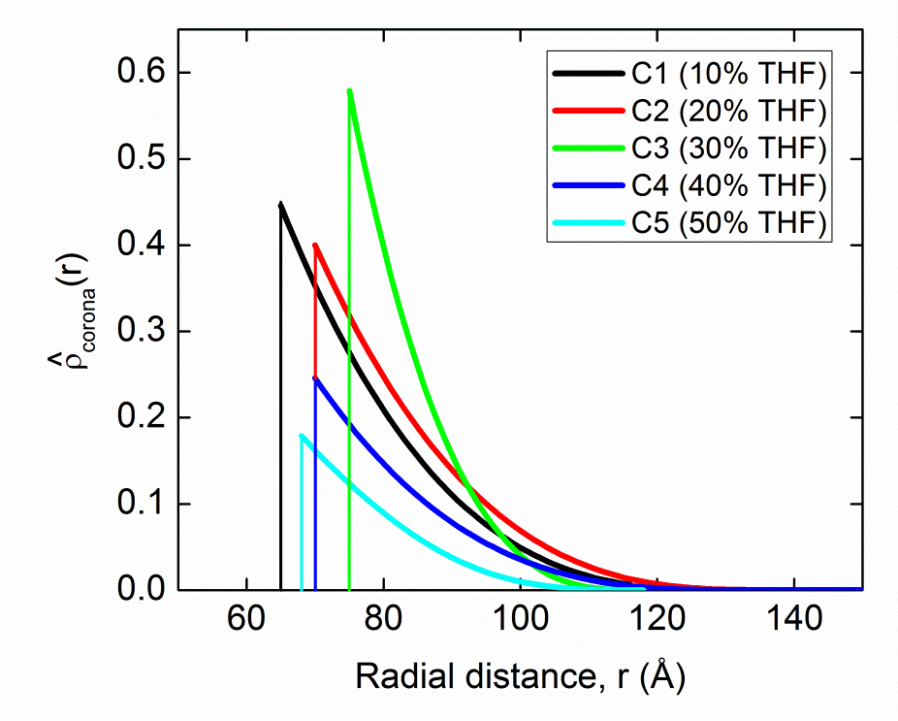

Figure 3.12. Rescaled corona density profiles for the samples of C series.

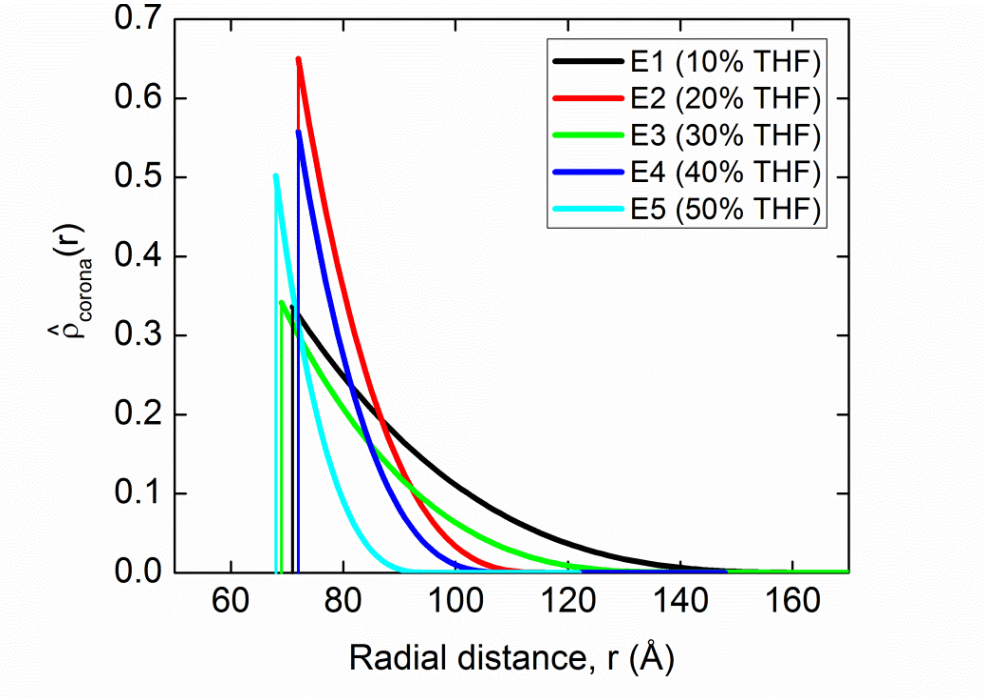

Figure 3.13. Rescaled corona density profiles for the samples of E series.

The micelle size was determined from the SANS corona profile and was truncated when the PEO chains reached a volume fraction of 0.02. This definition was used to calculate the micelle overall size (R_m) and the obtained R_m values are listed in the Tables 3.5 and 3.6. The width of the corona profile was calculated by taking the difference between the overall micelle size and the core radius ($H= R_m - R_c$), both calculated from SANS. The width of the corona profile continues to decrease steadily with increasing d-THF concentration in the C series, however, there is no specific trend in the E series. Similarly the overall micelle size, R_m, continues to decrease for the C series, however, the trend is varying in the E series, with increasing THF concentration. As the DLS results indicated an increase in the hydrodynamic radius with increasing THF content, we are currently trying to understand the origin of this discrepancy.

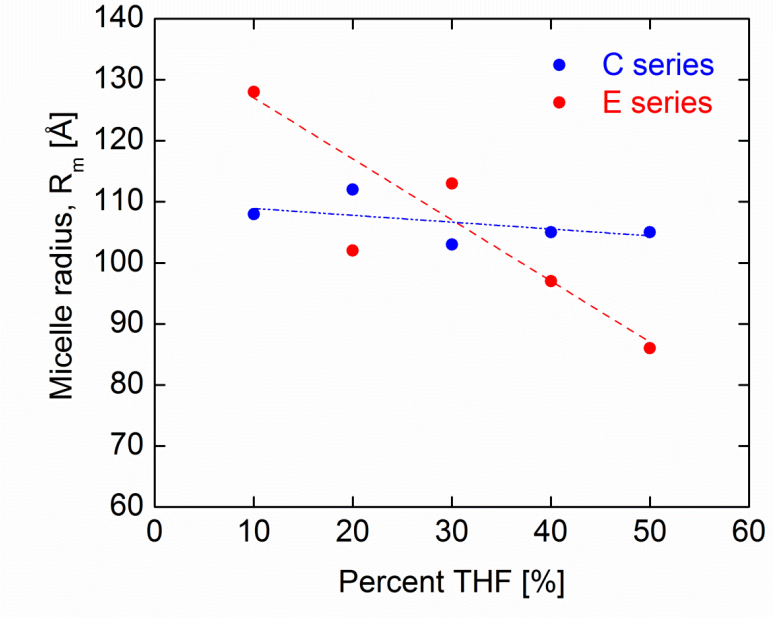

Figure 3.14. Micelle size (core + corona) for C and E series.

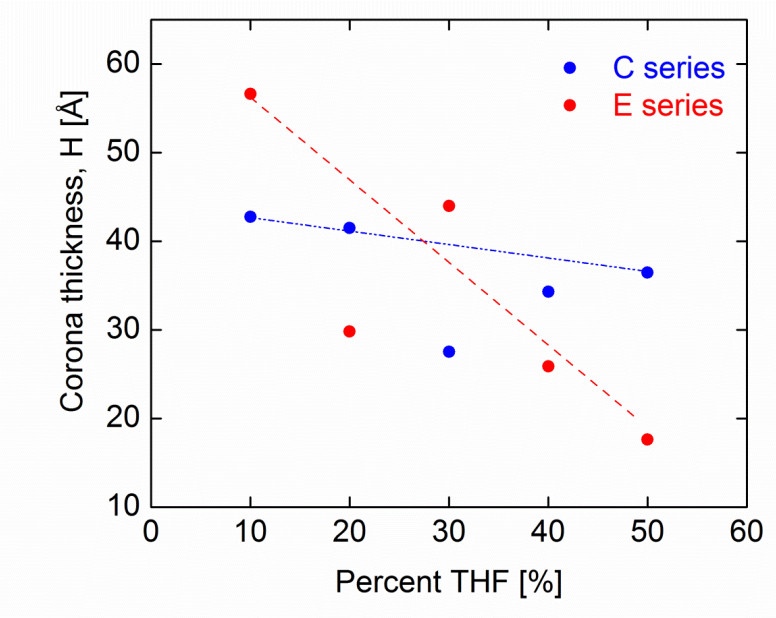

Figure 3.15. Corona thickness for C and E series.

Effect on polydisersity and the core-corona interfacial width*:* The polydisperisty in the size of micelles is increasing with increasing THF content. There is no definite trend observed in the interfacial width. We are still in the

process of making our fitting model to be more robust, and the observed trends might be different in that case.

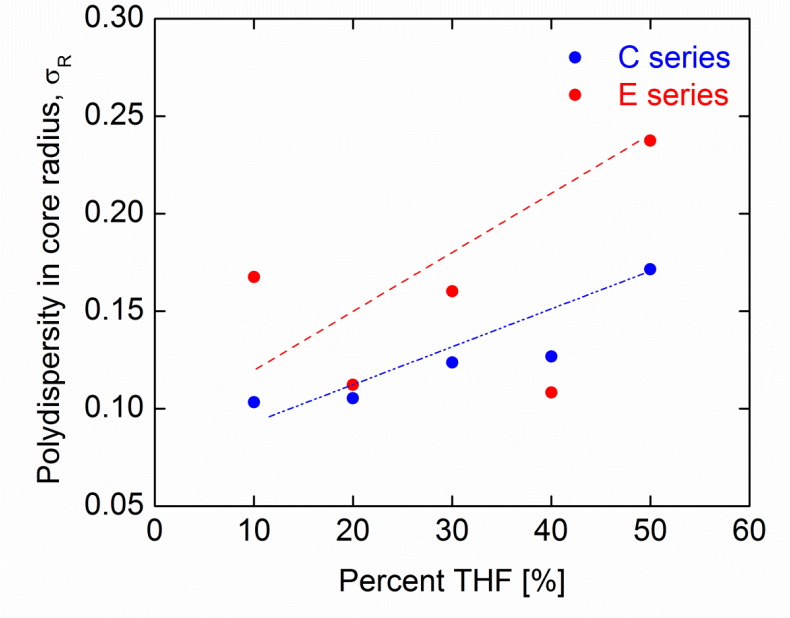

Figure 3.16. Polydispersity in core radius for C and E series.

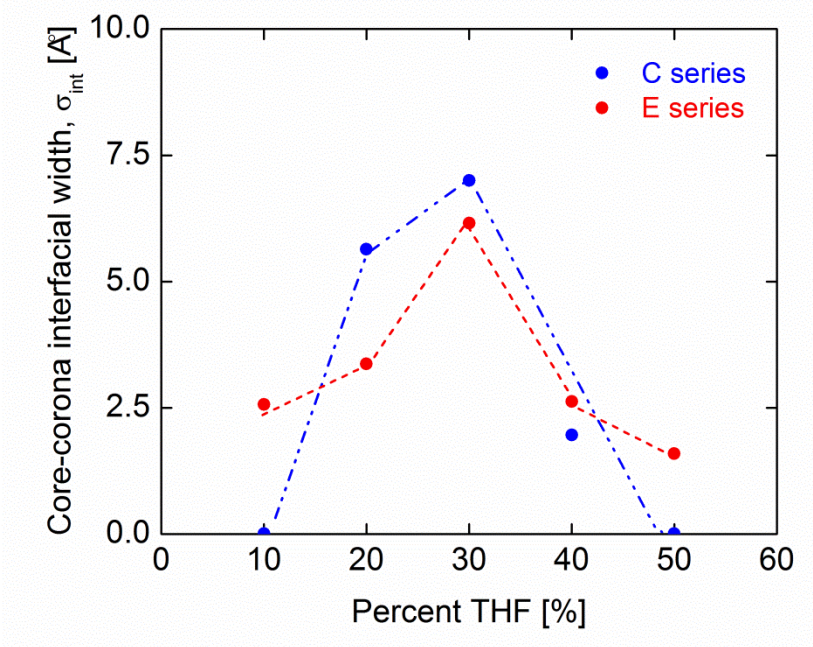

Figure 3.17. Core-corona interfacial width for C and E series.

3.5. Future work: simultaneous fitting of C, E and A-series

Additionally, in this data analysis, there are some discrepancies in the fitting between the C and E series, which we will address though the simultaneous fitting of the three micelle structures. Differences in micelle size as observed from DLS can be accounted for in the simultaneous fitting. The final goal is to fit the three different solvent compositions, and obtain critical information about micelle structural parameters, particularly if they are heavily swollen with the co-solvent. Figure 3.18 is a representative data set for the PEO_{2k}-PCL_{3k} micelle intensity profiles obtained the three different solvent compositions with the THF volume percent held at 40%.

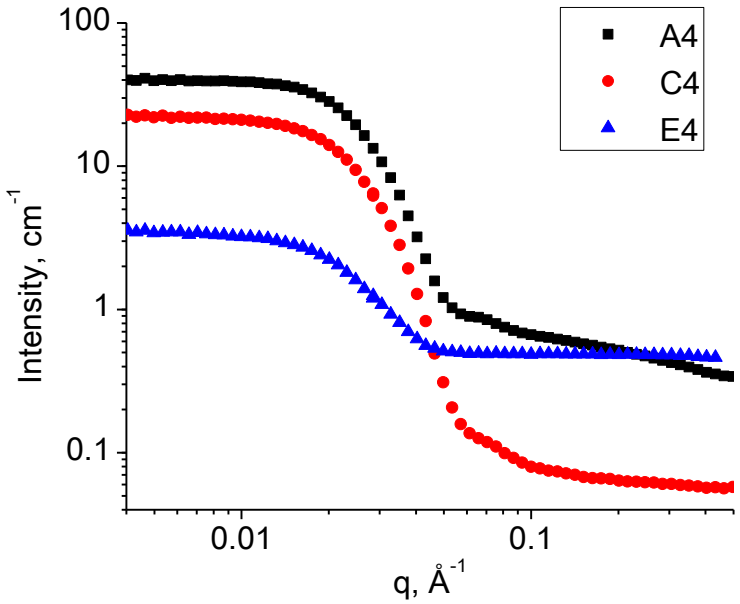

Figure 3.18. SANS intensity profiles for 40% THF in three different series.

Looking at the intensity profiles leads to an interesting observation in the low *q* intensities. Comparing scattering length densities of the solvent and the completely hydrogenated PEO-PCL block copolymer would indicate that C

series (dTHF/D_2O) would have the highest contrast, followed by A series (hTHF/D_2O) and the least contrast obtained in E series (h/d THF/ H_2O/D_2O). However, since the core is found be significantly swollen with the co-solvent, we see a surprising trend: the A-series has the highest low-q scattering, followed by the C-series, followed by the E-series. In this simple analysis we are assuming that the C and A series have the same degree of swelling of THF in the core; however, in the C series d-THF is used while in the A-series h-THF is used. The h- or d-THF is present not only in the core, but also in the bulk solvent. Based on Figure 3.18, the presence of d-THF in the core in the A-series actually reduces the contrast relative to the solvent mixture as compared to the contrast observed in the C-series. In the simultaneous fitting methods, these subtle differences in the scattering length densities of the core, corona and solvent will be accounted for. Global fitting parameters will be employed which are held constant across the three profiles, such as the aggregation number or conona parameters. The DLS results imply that there may be significant differences in the structural parameters and degree of swelling, based on the h and d content in the solvent. This will be explored in more detail in future work.

CHAPTER 4

DYNAMICS OF BLOCK COPOLYMER MICELLES

4.1. Time resolved-small angle neutron scattering (TR-SANS) concept

The basis of this technique is the difference in the scattering lengths of hydrogen (h) and deuterium (d). This difference gives rise to a contrast between the core of the micelle, and the solvent, which can be used to detect the exchange of chains between micelles at equilibrium. Two sets of polymeric micelles containing either hydrogenated PCL (h-PCL) or deuterated PCL (d-PCL) as the core polymer are prepared separately in a solvent whose scattering length density is matched to the average scattering length density of a 50/50 mixture of d-PCL and h-PCL. The two micelle solutions are mixed at t=0. As the h and d polymer chains exchange between micelles, the scattering intensity decreases over time (Figure 4.1).

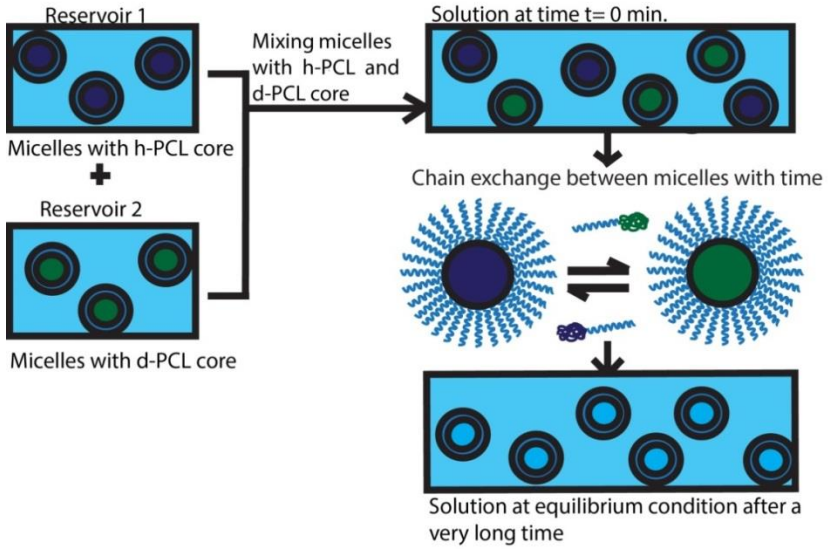

Figure 4.1. Schematic of a TR-SANS experiment.

Once the micelle cores contain equal numbers of h-PCL and d-PCL chains, there is no contrast with the solvent background, and the scattering becomes negligible.[18,3, 30]

For dilute systems, which have a low volume fraction of polymer, the SANS intensity $I(q)$ at any time depends on the contrast factor as following

$$I(q) \propto \left[\left(\frac{b(t)_{core}}{V_{core}}\right) - \left(\frac{b_{solvent}}{V_{solvent}}\right)\right]^2, \quad (4.1)$$

where, $b(t)_{core}/V_{core}$ is the time varying scattering length density of the core at any instant t, when the solution has mixed fractions of h-PCL and d-PCL, $b_{solvent}/V_{solvent}$ is the constant solvent (background) scattering length density, having contributions from H_2O and D_2O (in presence of THF, contributions proportionate to their volume fractions), and the PEO corona chains (which is ignored in this analysis).

SANS data is analyzed by examining the variation of $I(q)$ with respect to time. The chain exchange process can be quantified in time by a relaxation function which is defined in Equation 2.17.

The relaxation function for polymer micelles as predicted by Halperin and Alexander[25], to be a single exponential decay, is seldom encountered as shown below

$$R(t) = \exp(-kt). \quad (4.2)$$

In practice, distributions of relaxation processes are observed which can be explained by the polydispersity in the hydrophobic block length.[30-31] Therefore, a relaxation function can be defined as described in Equation 2.20. We performed three TR-SANS experiments, and they have similar experimental

procedures. For each experiment we will describe the information gained and conclusions, limitations of the experiments, and future directions.

4.2. Scattering length densities

Scattering length density (SLD) for thermal neutron cross sections are given as

$$SLD = \frac{\sum_{i=1}^{n} b_{c_i}}{V_m}, \quad (4.3)$$

where b_{c_i} is the bound coherent scattering length of ith of n atoms in a molecule with molecular volume V_m. The scattering length densities of different species are as given in Table 4.1.

Table 4.1. SLD's of different compounds and solvents.

Species	Molecular Formula	Mass Density @ 20 °C (g/cm^3)	Scattering Length Density (Å^{-2})
hCL	C6H10O2	1.15	8.48 x10^{-7}
dCL	C6H4D6O2	1.15	4.41 x10^{-6}
THF	C4H8O	0.889	1.84 x10^{-7}
H_2O	H2O	0.998	-5.59 x10^{-7}
D_2O	D2O	1.105	6.36 x10^{-6}
50/50 h/d CL	C6H7D3O2	1.15	2.68 x10^{-6}

4.3. Experiment 1

4.3.1. Experimental design

The characteristics of polymer samples used in experiment 1 are listed in Table 2.1. The first step in conducting any TR-SANS experiment is the determination of contrast match point. Micelle solutions were prepared in water / tetrahydrofuran (THF) mixtures, where the THF content varied as 0, 10 and 20 vol.%. Since micelles are sometimes frozen in the selective solvent, the co-dissolution of a good solvent is often required. The measurements were

conducted 60°C above the melting point of PCL polymer to exclude any effect of core crystallization.

Contrast matching for TR-SANS: Contrast matching experiments were conducted on micelles with a 50/50 mixture of h and d polymers in the core. Premixed micelle solutions (containing 50/50 amounts of h/d polymers weighed together during the micelle preparation procedure) were prepared in various solvent compositions. For each solvent composition (at a fixed THF: (H_2O + D_2O) ratio), the concentration of THF was held constant, and the ratio of H_2O to D_2O was varied (Figure 4.2).

The integral of the intensity was calculated and plotted against the volume fraction of D_2O. The contrast matched solvent composition has the same neutron scattering length density as the core. For the data illustrated in Figure 4.2, the contrast matched solvent conditions were found to be: 54% H_2O / 26% D_2O / 20% THF (Figure 4.3).

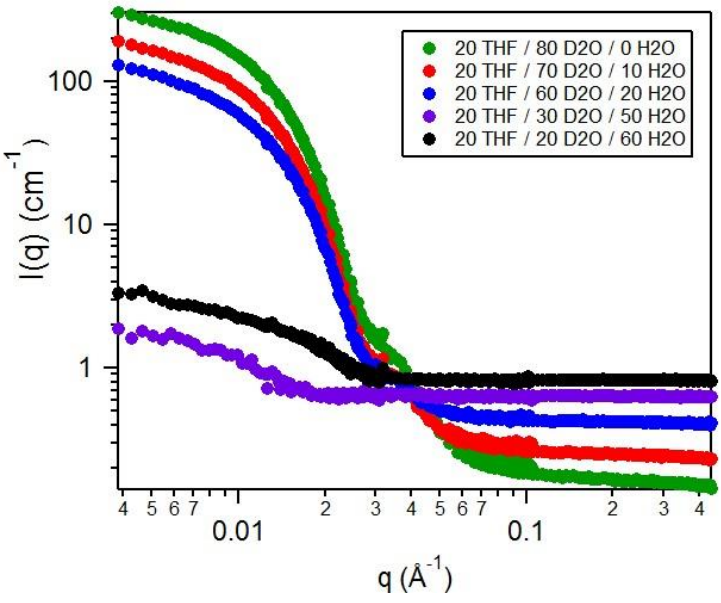

Figure 4.2. Intensity profile for different ratios of H_2O/D_2O for 20 vol% THF.

Here, the volume fraction of D_2O was determined at which I(q) went to zero, indicating the contrast match composition (the first data point was reflected through the intensity axis for a clear determination of the contrast match point).

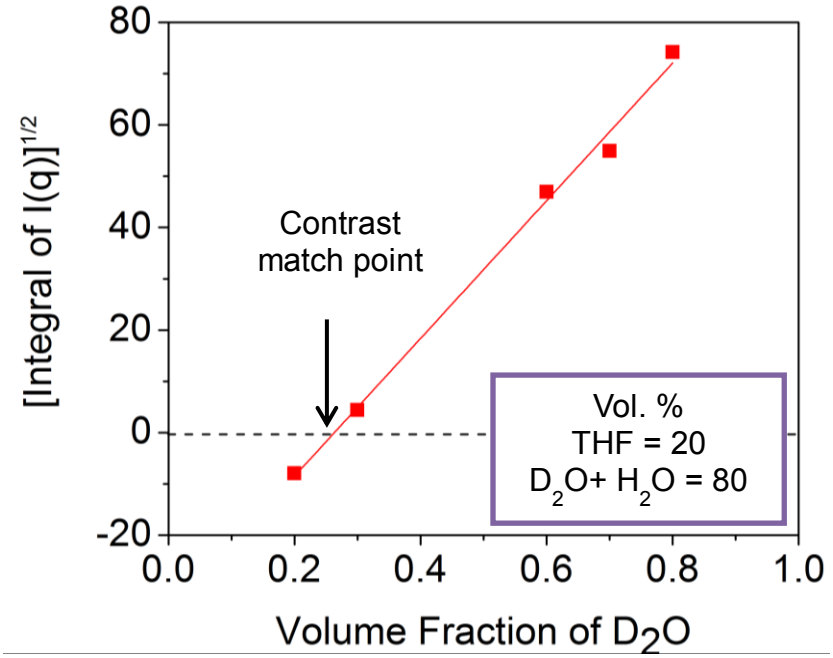

Figure 4.3. Contrast match point determination for 20% vol THF.

4.3.2. Results of Experiment 1

4.3.2a) Presence of solvent in the core

Comparing the SLD of the contrast match solvent conditions with the SLD of a 50/50 h/d mixed core (without any solvent present in the core), we found a significant discrepancy in the two values. It can be explained by the presence of cores swollen with solvent, as the added co-solvent (good solvent for both the blocks) will penetrate the core region. Estimating the amount of solvent present in the core, by matching with the SLD of the contrast match

conditions, indicated heavy swelling with THF (Table 4.4). For the 20% volume THF samples, it was approximately 52 vol.% of the core. Similar observations were made by the Epps group[6c], where they determined the volume fraction of the co-solvent in the core to be considerably higher than the bulk composition.

Table 4.2. Comparison of SLDs of the swollen micelle core

Sample	Scattering Length Density ($Å^{-2}$)
THF	1.84×10^{-7}
D_2O	6.37×10^{-7}
H_2O	-5.60×10^{-7}
54% H_2O / 26% D_2O / 20% THF	1.39×10^{-6}
Core containing 52% THF	1.38×10^{-6}

4.3.2b) Structural properties of h and d micelles

Though the prepared diblock copolymers have similar molecular weights and compositions, it is essential to determine if the prepared micelles have similar structures, and hence, they should be characterized by SANS before the TR-SANS experiment to determine kinetics. Figure 4.4 illustrates the minor differences when both the h and d labeled polymers were prepared in the contrast matched solvent. The black curve indicates the scattering from the premixed micelle core (contains 50/50 h/d polymer in the core) prepared in the contrast matched solvent, indicating little contrast between the micelles and solvent when there is a 50/50 mixture of h and d polymers in the core. Incoherent scattering of the solvent is indicated by the dashed line on the plot.

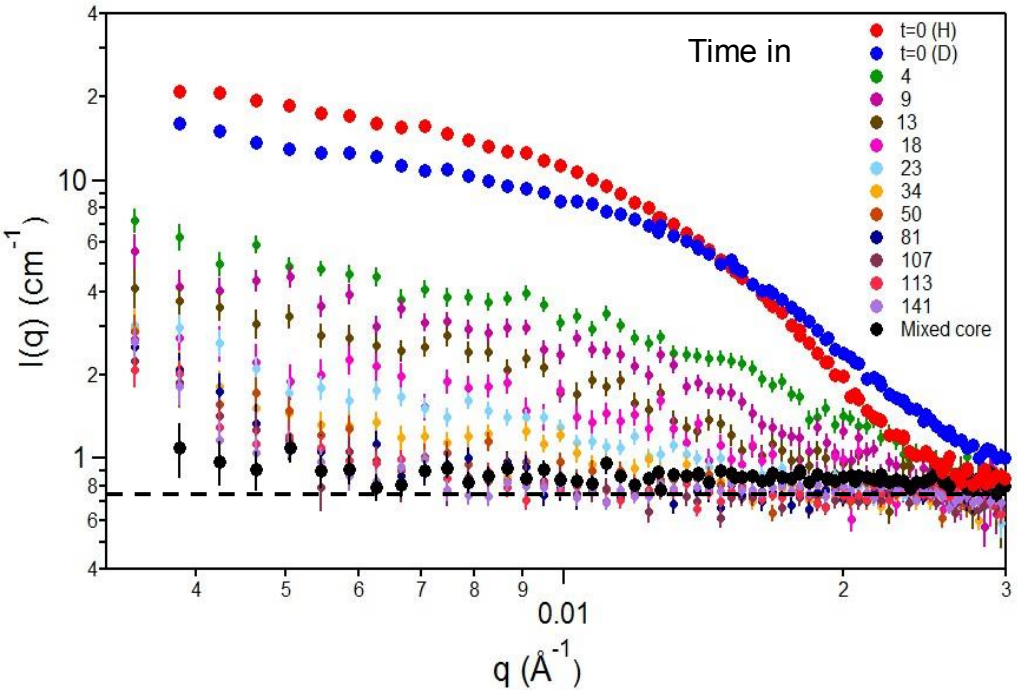

Figure 4.4. Intensity change with time as monitored through the SANS instrument.

4.3.2c) Data analysis and discussion

The SANS intensity is proportional to the scattering length density difference between the micelle core and solvent, and as h and d polymers exchange between the micelle cores, the contrast decreases over time and hence the overall intensity also reduces. In a little over two hours, the sample containing 20% THF contains 50/50 h/d cores, such that the resulting intensity is now matched to that expected from the incoherent scattering of the solvent (or alternatively, the premixed micelle sample). Though the TR-SANS intensity became negligibleover 2 hours for 20% THF samples, the samples containing 10% THF showed minor decreases over 3 hours, indicating a much slower change rate when the THF content is reduced. Furthermore, no change was

detected in scattering from the micelle solutions prepared at 0% THF, indicating the presence of completely frozen micelles (i.e. lack of chain exchange).

The absolute intensity in SANS depends on both the contrast and the structure of micelles. Since the structure of the micelles is not changing in this dynamic process (they are not disintegrating), the intensity only depends on the contrast[30]: Here $\frac{b_{solvent}}{V_{solvent}}$ is determined by the solvent composition (and includes a small contribution from the corona chains), and does not change in a TR-SANS experiment. The $\frac{b(t)_{core}}{V_{core}}$ term is the scattering length density of the core, influenced by the presence of either h or d chains, and the difference in scattering length densities changes over time until the cores contain completely mixed h and d chain in the core.

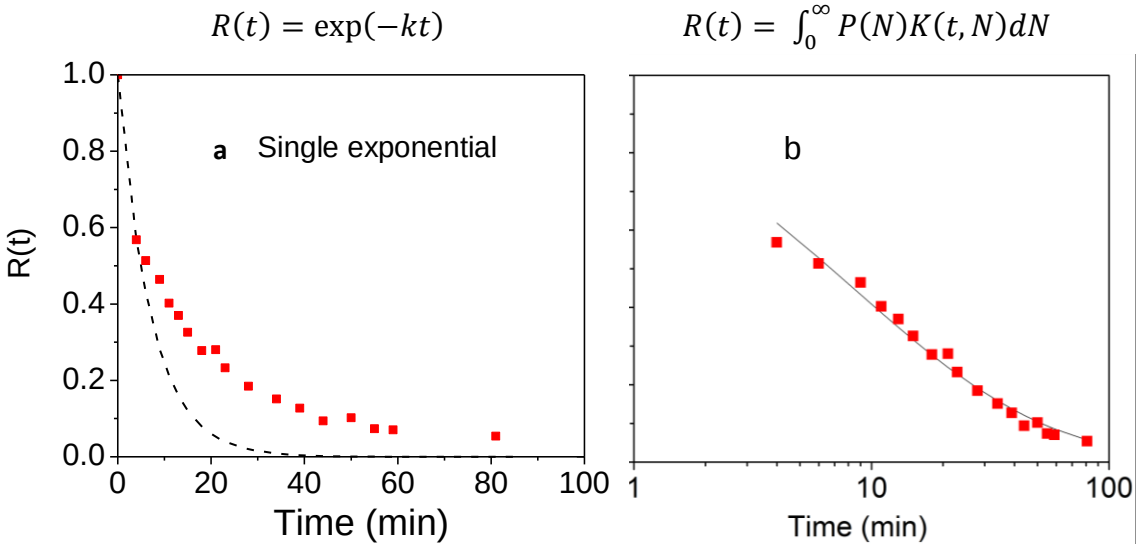

Figure 4.5: a) Relaxation function fit with a single exponential function and b) Relaxation function fit to the detailed model by Choi et al.[2b],using the concentration flux function.

The relaxation function, $R(t)$, describes the reduction of the scattering intensity over time during the TR-SANS experiments (Equation 2.17). $R(t)$ is plotted below against log t, for measurements conducted at 60 °C (Figure 4.5). The temperature was raised above the melting point of PCL to enable faster chain exchange to be measured in relevant time scales[3]. From the intensity profile at different times, we note that the decay is faster in the beginning and then slows down. Consistent with literature[3, 30-31], the single exponential fit to this data as predicted by Halperin and Alexander[25] is a poor fit (Figure 4.5a), and instead, our relaxation function also had linear dependence with logarithmic time scale, similar to that observed in Choi et al.[30] (Figure 4.5b).

A possible explanation for broad relaxation times observed in polymer micelles was initially thought to be concerted mechanisms for the rate limiting chain expulsion step. However, there were no effects of the polymer concentration on the chain exchange dynamics[3]. Diffusion of the chain through the solvent also does not play any role in chain kinetics as the diffusion time between micelles is estimated to be of the order of microseconds[3], whereas the expulsion rate is much slower, on the order of minutes.

There are three main processes involved in a chain exchange from one micelle to another[3, 26a, 30]:

1) Expulsion of a unimer from a micelle core.
2) Movement through the solvent when it has unfavorable core block-solvent interactions.
3) Insertion into another micelle.

Higher order chain kinetic processes such as fission and fusion are ignored in this analysis. Of the above three steps, the first one is considered to the most energy intensive, and therefore, is the rate limiting one. The net core block flux, of either the h or the d chains, depends on the concentration gradient[30]

$$\frac{c(t)-c(0)}{c(\infty)-c(0)} = \exp\left(\frac{-t}{\Gamma(N)}\right), \tag{4.4}$$

where $\Gamma(N)$ is the characteristic exchange time. It is approximated by the longest (Rouse) relaxation time for un-entangled polymer melts, and is given by

$$\Gamma_{Rouse} = \frac{N^2 b^2 \zeta}{6\pi^2 k_B T}, \tag{4.5}$$

where k_B, T, b, ζ are the Boltzman constant, temperature, statistical segment length and the monomeric friction factor respectively.

Due to swelling of the core (as determined from contrast matching analysis and literature), we expected our core block polymer to be un-entangled as well. Choi et al. accounted for the extraction of core block not only in regard to the expulsion of a chain from the micellar core but also for the thermodynamically unfavorable core block solvent interactions as it comes out of the core block[30]. Consequentially, there is additional penalty for a chain expulsion, such that the concentration flux function is modified as defined in Equation 2.18. In this expression, we note that $K(t,N)$ depends on the double exponential of the N, therefore even a small polydispersity will have huge effect on $K(t,N)$. The polydispersity in the core block is accounted by a Gaussian

distribution function as described in Equation 2.19. The final relaxation function is given by Equation 2.20.

These set of equations were used to analyze the data shown in Figure 4.5a. The monomeric friction factor was used from literature[39] and the statistical segment length b was estimated using C-C and C-O bond lengths in PCL. The value of b used was 10.56 Å. These equations have been used to fit the relaxation function data shown in Figure 4.5b. From the fit, the value of $\alpha\chi$ is 0.47 which is close to what one would expect for the interactions between a strongly hydrophobic block (PCL) and water.

4.3.3. Conclusions of Experiment 1

TR-SANS indicated the presence of chain exchange between the PEO_{2k}-PCL_{4k} micelles in THF/D_2O/H_2O. THF addition enhanced the rates of chain exchange by reducing the interfacial tension with the PCL core. SANS data was fitted using the relaxation function developed by Choi et al.[3030], which considered the additional unfavorable interaction of the core block with solvent in the chain exchange process and reasonable core block-solvent interaction parameter values was obtained.

4.3.4. Future work directions

Though the data analysis broadly agrees with the expected outcomes from literature, we had some concerns about the integrity of our samples. Our polymer micelle solutions were most likely phase separated as the very low q range was marked by a sharp upturns, indicating presence of large aggregates. Visually, the samples turned cloudy on cooling from 60°C to room

temperatures. Cloudiness implies phase separation on the micro-scale phase separation. Also based on literature, the relaxation function is very sensitive to the polydisersity of the core block polymer. The polymers used in this experiment were relatively broad in their molecular weight distribution (PDI >1.5). For the next experiment, we aimed to synthesize polymers with narrower polydispersity, and special care was taken to select samples whose micelle solutions were clear upon preparation.

4.4. Experiment 2

4.4.1. Experimental design for Experiment 2

Two sets of narrow PEO-PCL polymers were prepared (Polymers A and B), whose characteristics are listed in Table 2.1. The smaller PCL weight fraction h/d pair was synthesized to see the effect of core block length on the chain kinetics. The micelle solutions prepared using these polymers were clear in appearance and easy to filter. DLS data also indicated unimodal decay of autocorrelation function signifying that there was no phase separation in these solutions. Micelles were again prepared in water /THF mixtures, where the THF content was varied as 0%, 10% and 20% for each of the diblock copolymers. Micelles solutions were sonicated at the neutron facility after shipping to break any loose aggregates that might have formed over time. The SANS measurement were again conducted at 60°C. The solvent match point compositions obtained by contrast matching were in close proximity to the match point conditions as obtained before in Experiment 1.

4.4.2. Results of Experiment 2

The resulting h and d labeled core polymer prepared in the contrast matched solvent compositions had very low intensities. One example is shown in Figure 4.6. There were also differences in the intensities at t=0, but comparing with the t=0 data collected, for h and d polymer profiles, in Experiment 1, they were the same magnitude of difference. Also, these experiments were conducted at a high temperature, 60 °C for measuring chain exchange over a reasonable amount of time, but in this case, the intensity changed too quickly to be measured reliably. Estimating the amount of the solvent present in the core, by comparing the contrast match point indicated heavy swelling of the micelle cores as found in the last experiment. The intensities observed in this experiment were incredibly low, close to the solvent background, limiting our ability to make strong conclusions from this data.

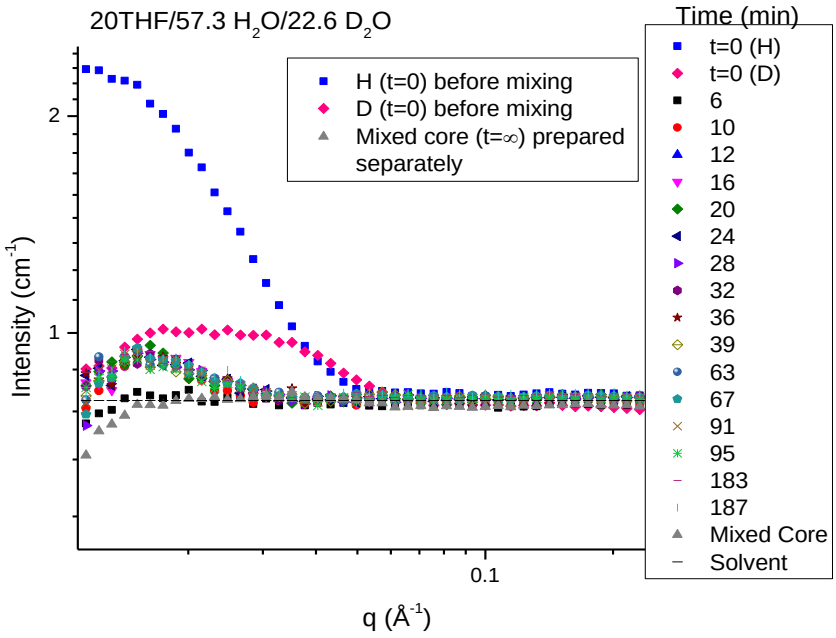

Figure 4.6. TR-SANS intensities collected for PEO_{2k}-PCL_{3k} polymeric micelles in 20%THF.

To address the issue of the low intensities observed, we using freeze drying to isolate the polymer from the solvent in one of the contrast match samples. Then NMR experiments were used to verify the ratio of h and d polymers in the contrast match sample. . It was determined that this contrast match samples had approximately the expected ratio of H and D atoms for the 50/50 mixed core. The analysis is presented below for this NMR calculation. The structure of h and d PCL repeat unit are shown in Figures 4.7 a and b respectively.

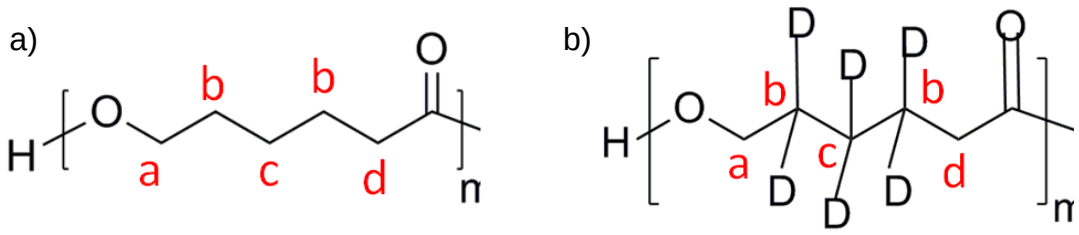

Figure 4.7. a) Structure of h PCL and b) structure of d PCL.

Table 4.3. NMR analysis on polymer PEO_{2k}-$hPCL_{2k.}$

Index	Peak Location (ppm)	Obtained peak ratios w.r.t. peak 'a' (hPCL)
a	4.05	1.00
b	1.65	2.10
c	1.30	1.05
d	2.30	1.06

Table 4.4. NMR analysis on polymer PEO_{2k}-$dPCL_{2k.}$

Index	Peak Location (ppm)	Obtained peak ratios w.r.t. peak 'a' (dPCL)
a	4.05	1.00
b	1.65	$0.27^{\Phi 1}$
c	1.30	$0.15^{\Phi 2}$
d	2.30	1.02

$^{\Phi}$Note: Some percentage of atoms are undeuterated. $^{\Phi 1}$13% atoms undeuterated. $^{\Phi 2}$15% atoms undeuterated.

Table 4.5. NMR performed on 50/50 h/d micelle solution used in contrast matching.

Index	Peak Location (ppm)	Expected peak ratios-w.r.t. 'a' (50/50 h/d PCL)[#]	Obtained peak areas in contrast matched sample[#]	Obtained peak ratios-w.r.t. 'a' (contrast matched sample)[#]
a	4.05	1.00	18.72	1.00
b	1.65	1.19	26.07	1.39
c	1.3	0.60	10.57	0.56
d	2.3	1.04	19.42	1.04

[#]Micelle solution containing 20% THF was freeze-dried prior to performing NMR

Table 4.6. Percentage of h/d in the contrast matched sample.

Fraction h	Fraction d
0.45	0.55

4.4.3. Conclusions of Experiment 2 and directions for future work

The micelles used in Experiment 2 had very low polydispersities and well-controlled characteristics. Unfortunately, although chain exchange was detected in all solvent compositions, it occurred too quickly to be measured reliably. There were additional limitations due to SANS intensities from these micelle solutions. The reason for this is that in Experiment 1, we determined that there was macrophase separation of the micelle solution, which greatly increased the overall scattering intensities. In Experiment 2 we prepared well-controlled micelle solutions that did not phase separate, and the SANS intensities were much lower. An additional factor is that the micelle cores were heavily swollen with the solvent, further reducing the contrast between the core and the solvent. We used a core-shell model to predict the effect of the micelle size on the intensity profile, using a swollen core, which indicated that increasing the size of the core would increase the intensities (Figure 4.9).

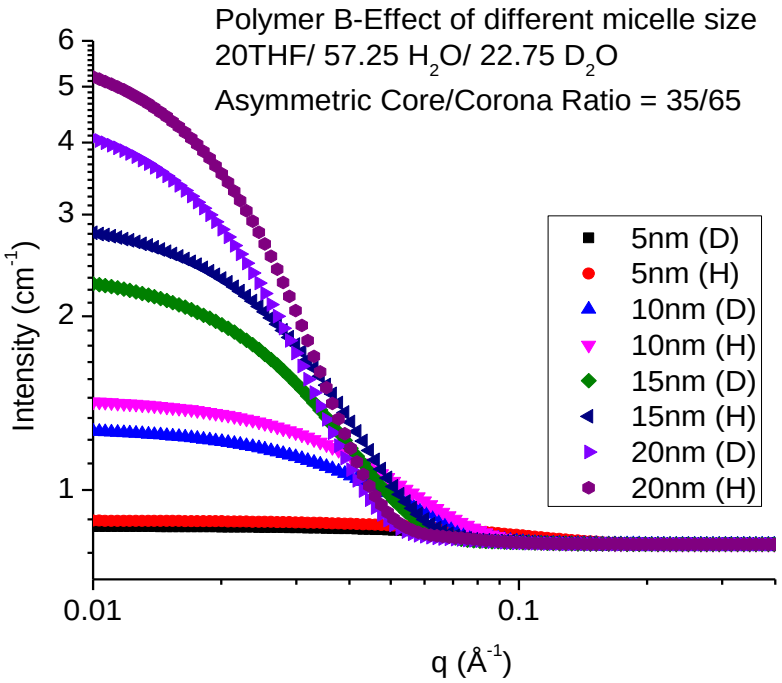

Figure 4.8. Intensity predictions using the core-shell model for different micelle sizes.

Therefore, we decided to synthesize narrow PEO-PCL (M_n PEO= 5 kg/mol) polymers for micelle preparation. Additionally, experiments conducted at room temperature, instead of 60°C, would in theory reduce the rate of chain exchange and increase the micelle size, based on DLS experiments.

4.5. Experiment 3

4.5.1. Experimental design for Experiment 3

Micelle solutions were prepared from Polymer B of the last experiment and a high molecular weight analogue was prepared, Polymer C (PEO_{5k}-PCL_{5k}), whose characteristics are listed in Table 2.1.The micelle solutions were clear in appearance, easy to filter and DLS indicated no phase separation and an almost uniform micelle size. Micelle solutions were prepared in four different

water / tetrahydrofuran (THF) mixtures, where the THF content was varied as 0%, 5%, 10% and 20 vol. %. The measurements were conducted at room temperature this time to slow down the kinetics of chain exchange which was observed at elevated temperatures, as well as increase the micelle size and resulting intensities.

4.5.2. Results of Experiment 3

The contrast matched conditions were again found to be in good agreement with the previously determined match point conditions but, increasing the size of polymer had very small effect on absolute intensity.

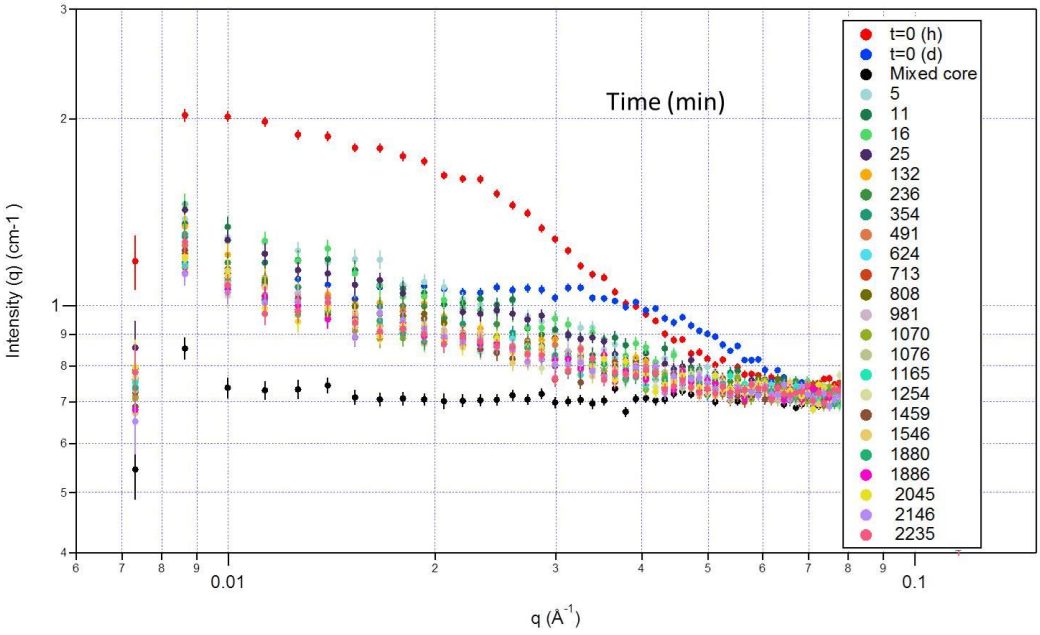

Figure 4.9. The decrease in intensity for PEO_{2k}-PCL_{3k} micelle solutions in 10%THF.

The overall contrast is hypothesized to be dominated by the core being swollen with solvent, which reduces the contrast between the core and solvent. Also, the intensities did not decrease to the contrast matched sample for the TR-

SANS solutions (Figure 4.10). DLS measurements indicate some minor difference in micelle sizes for those containing h-PCL vs. d-PCL (Figure 4.11).

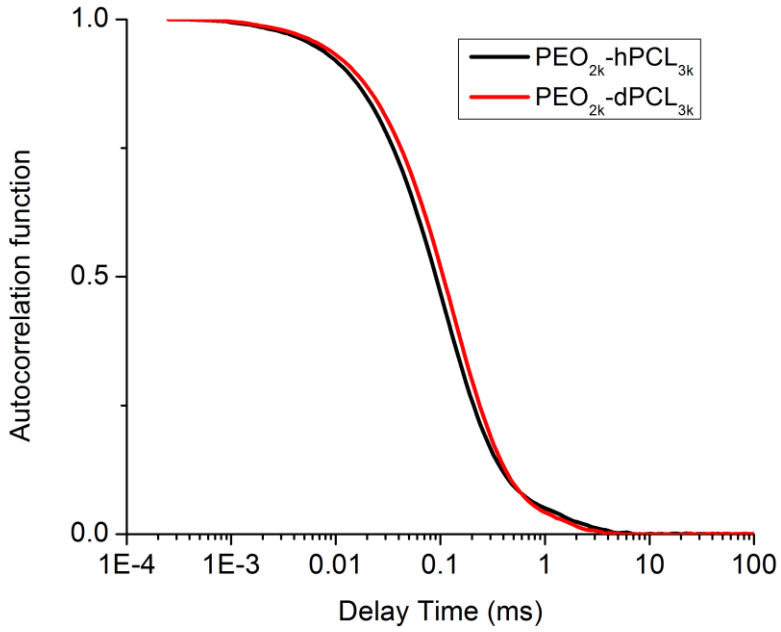

Figure 4.10. Micelle solutions prepared in 20% THF composition. PEO_{2k}-$hPCL_{3k}$ sample is prepared in 20%THF/80 %H_2O and PEO_{2k}-$dPCL_{3k}$ sample is prepared in 20%THF/80% D_2O.

4.5.3. Conclusions from Experiment 3 and directions for future work

Chain exchange was observed at relatively slower time scales and increasing the length of hydrophobic block reduced the rate of chain exchange. However, most samples (except for PEO_{2k}-PCL_{3k} micelle solution in 20% THF) did not reach the completely mixed core scattering profile. In future experiments, we need to verify if the polymer concentrations are different in the h and d micelle solution due to the isotope effect. For this, we need to characterize the concentration of h and d polymer separately in every micelle solution, using freeze drying and NMR technques, as there can be differences

in the solubility of h/d micelles, which could explain intensities not matching those of the premixed core. Also, in order to improve the contrast, we will use a completely deuterated core polymer instead of partially deuterated PCL. the fully deuterated monomer has recently been supplied by the Center for Nanophase Materials Sciences at Oak Ridge National Lab.

CHAPTER 5

CONCLUSIONS

We investigated the effect of co-solvent variation on the micelle structural properties and their dynamics, using the neutron scattering experiments. Critical structural parameters were extracted by fitting a detailed micelle form factor model to the intensity profiles obtained from SANS. Information such as the aggregation number, percent THF in the core, micelle core radius, and thickness of the corona can be obtained from the fitted curves. An important consideration was the calculation of scattering length of the core based on the amount of THF weight fraction present in the core, which was a fitting parameter. There were definite trends in aggregation number and percent THF in the core. Aggregation number was found to be decreasing while the degree of swelling of the core was found to be higher with increasing THF content of the solvent. The next step will be to try the simultaneous fitting across the three solvent compositions taking into account their structural differences.

THF addition also has a profound effect on the rates of chain exchange by reducing the interfacial tension with the PCL core. TR-SANS indicated faster kinetics of chain exchange with increasing THF content in the solvent. In the future, we will conduct TR-SANS experiments with improved core-solvent contrast and establish the characteristics time scales of with changing THF ratios.

REFERENCES

1. Riess, G., "Micellization of block copolymers." *Progress in Polymer Science* **2003,** *28* (7), 1107-1170.

2. Patist, A.; Kanicky, J. R.; Shukla, P. K.; Shah, D. O., "Importance of Micellar Kinetics in Relation to Technological Processes." *Journal of Colloid and Interface Science* **2002,** *245* (1), 1-15.

3. Lund, R.; Willner, L.; Richter, D.; Dormidontova, E. E., "Equilibrium Chain Exchange Kinetics of Diblock Copolymer Micelles: Tuning and Logarithmic Relaxation." *Macromolecules* **2006,** *39* (13), 4566-4575.

4. (a) Choucair, A.; Lavigueur, C.; Eisenberg, A., "Polystyrene-b-poly(acrylic acid) Vesicle Size Control Using Solution Properties and Hydrophilic Block Length." *Langmuir* **2004,** *20* (10), 3894-3900; (b) Zhang, L.; Bartels, C.; Yu, Y.; Shen, H.; Eisenberg, A., "Mesosized Crystal-like Structure of Hexagonally Packed Hollow Hoops by Solution Self-Assembly of Diblock Copolymers." *Physical Review Letters* **1997,** *79* (25), 5034-5037; (c) Zhang, L.; Eisenberg, A., "Thermodynamic vs Kinetic Aspects in the Formation and Morphological Transitions of Crew-Cut Aggregates Produced by Self-Assembly of Polystyrene-b-poly(acrylic acid) Block Copolymers in Dilute Solution." *Macromolecules* **1999,** *32* (7), 2239-2249; (d) Zhang, L.; Eisenberg, A., "Structures of “crew-cut” aggregates of polystyrene-b-poly(acrylic acid) diblock copolymers." *Macromolecular Symposia* **1997,** *113* (1), 221-232.

5. Zhang, L.; Yu, K.; Eisenberg, A., "Ion-Induced Morphological Changes in “Crew-Cut” Aggregates of Amphiphilic Block Copolymers." *Science* **1996,** *272* (5269), 1777-1779.

6. (a) Abbas, S.; Li, Z.; Hassan; Lodge, T. P., "Thermoreversible Morphology Transitions of Poly(styrene-b-dimethylsiloxane) Diblock Copolymer Micelles in Dilute Solution." *Macromolecules* **2007,** *40* (11), 4048-4052; (b) Mihut, A. M.; Drechsler, M.; Möller, M.; Ballauff, M., "Sphere-to-Rod Transition of Micelles formed by the Semicrystalline Polybutadiene-block-Poly(ethylene oxide) Block Copolymer in a Selective Solvent." *Macromolecular Rapid Communications* **2010,** *31* (5), 449-453; (c) Kelley, E. G.; Smart, T. P.; Jackson, A. J.; Sullivan, M. O.; Epps, T. H., "Structural changes in block copolymer micelles induced by cosolvent mixtures." *Soft Matter* **2011,** *7* (15), 7094-7102; (d) Bang, J.; Viswanathan, K.; Lodge, T. P.; Park, M. J.; Char, K., "Temperature-dependent micellar structures in poly(styrene-b-isoprene) diblock copolymer solutions near the critical micelle temperature." *The Journal of Chemical Physics* **2004,** *121* (22), 11489-11500.

7. Lund, R.; Willner, L.; Stellbrink, J.; Radulescu, A.; Richter, D., "Role of Interfacial Tension for the Structure of PEP−PEO Polymeric Micelles. A Combined SANS and Pendant Drop Tensiometry Investigation." *Macromolecules* **2004,** *37* (26), 9984-9993.

8. Lund, R.; Pipich, V.; Willner, L.; Radulescu, A.; Colmenero, J.; Richter, D., "Structural and thermodynamic aspects of the cylinder-to-sphere transition in amphiphilic diblock copolymer micelles." *Soft Matter* **2011,** *7* (4), 1491-1500.

9. (a) Halperin, A., "Polymeric micelles: a star model." *Macromolecules* **1987,** *20* (11), 2943-2946; (b) Svaneborg, C.; Pedersen, J. S., "Form Factors of Block Copolymer Micelles with Excluded-Volume Interactions of the Corona Chains Determined by Monte Carlo Simulations." *Macromolecules* **2001,** *35* (3), 1028-1037; (c) Pedersen, J. S.; Svaneborg, C., "Scattering from block copolymer micelles" *Curr. Opin. Colloid Interface Sci.* **2002,** *7*, 158; (d) Svaneborg, C.; Pedersen, J. S., "A Monte Carlo study on the effect of excluded volume interactions on the scattering from block copolymer micelles." *J. Chem. Phys.* **2000,** *112*, 9661; (e) Svaneborg, C.; Pedersen, J. S., "Block copolymer micelle coronas as quasi-two-dimensional dilute or semidilute polymer solutions." *Phys. Rev. E* **2001,** *64*, 010802; (f) Alexander, S., "Polymer adsorption on small spheres. A scaling approach" *J. Phys. (Paris)* **1977,** *38*, 977.

10. (a) Pedersen, J., "Form factors of block copolymer micelles with spherical, ellipsoidal and cylindrical cores." *Journal of Applied Crystallography* **2000,** *33* (3 Part 1), 637-640; (b) Pedersen, J. S., "Structure factors effects in small-angle scattering from block copolymer micelles and star polymers." *The Journal of Chemical Physics* **2001,** *114* (6), 2839-2846; (c) Pedersen, J. S.; Gerstenberg, M. C., "The structure of P85 Pluronic block copolymer micelles determined by small-angle neutron scattering." *Colloids and Surfaces A: Physicochemical and Engineering Aspects* **2003,** *213* (2–3), 175-187; (d) Pedersen, J. S.; Gerstenberg, M. C., "Scattering Form Factor of Block Copolymer Micelles." *Macromolecules* **1996,** *29* (4), 1363-1365; (e) Pedersen,

J. S.; Hamley, I. W.; Ryu, C. Y.; Lodge, T. P., "Contrast Variation Small-Angle Neutron Scattering Study of the Structure of Block Copolymer Micelles in a Slightly Selective Solvent at Semidilute Concentrations." *Macromolecules* **1999,** *33* (2), 542-550.

11. Castelletto, V.; Hamley, I. W.; Pedersen, J. S., "A small-angle neutron scattering investigation of the structure of highly swollen block copolymer micelles." *The Journal of Chemical Physics* **2002,** *117* (17), 8124-8129.

12. Aniansson, E. A. G.; Wall, S. N.; Almgren, M.; Hoffmann, H.; Kielmann, I.; Ulbricht, W.; Zana, R.; Lang, J.; Tondre, C., "Theory of the kinetics of micellar equilibria and quantitative interpretation of chemical relaxation studies of micellar solutions of ionic surfactants." *The Journal of Physical Chemistry* **1976,** *80* (9), 905-922.

13. Wennerström, H.; Lindman, B., Micelles. "Physical chemistry of surfactant association." *Physics Reports* **1979,** *52* (1), 1-86.

14. Mok, M. M.; Thiagarajan, R.; Flores, M.; Morse, D. C.; Lodge, T. P., "Apparent Critical Micelle Concentrations in Block Copolymer/Ionic Liquid Solutions: Remarkably Weak Dependence on Solvophobic Block Molecular Weight." *Macromolecules* **2012,** *45* (11), 4818-4829.

15. Nyrkova, I. A.; Semenov, A. N., "On the Theory of Micellization Kinetics." *Macromolecular Theory and Simulations* **2005,** *14* (9), 569-585.

16. (a) Won, Y.-Y.; Davis, H. T.; Bates, F. S., "Molecular Exchange in PEO−PB Micelles in Water." *Macromolecules* **2003,** *36* (3), 953-955; (b) Stejskal, J.; Hlavatá, D.; Sikora, A.; Konňák, Č.; Pleštil, J.; Kratochvíl, P.,

"Equilibrium and non-equilibrium copolymer micelles: polystyrene-block-poly (ethylene-co-propylene) in decane and in diisopropylether." *Polymer* **1992,** *33* (17), 3675-3685; (c) Schouten, M.; Dorrepaal, J.; Stassen, W. J. M.; Vlak, W. A. H. M.; Mortensen, K., "Thermal stability of polystyrene-b-poly(ethylene/propylene) diblock copolymer micelles in paraffinic solvents." *Polymer* **1989,** *30* (11), 2038-2046.

17. (a) Jain, S.; Bates, F. S., "Consequences of Nonergodicity in Aqueous Binary PEO−PB Micellar Dispersions." *Macromolecules* **2004,** *37* (4), 1511-1523; (b) Meli, L.; Santiago, J. M.; Lodge, T. P., "Path-Dependent Morphology and Relaxation Kinetics of Highly Amphiphilic Diblock Copolymer Micelles in Ionic Liquids." *Macromolecules* **2010,** *43* (4), 2018-2027.

18. Willner, L.; Poppe, A.; Allgaier, J.; Monkenbusch, M.; Richter, D., "Time-resolved SANS for the determination of unimer exchange kinetics in block copolymer micelles." *EPL (Europhysics Letters)* **2001,** *55* (5), 667.

19. Cui, H.; Chen, Z.; Zhong, S.; Wooley, K. L.; Pochan, D. J., "Block Copolymer Assembly via Kinetic Control." *Science* **2007,** *317* (5838), 647-650.

20. (a) Jones, M.-C.; Leroux, J.-C., "Polymeric micelles – a new generation of colloidal drug carriers." *European Journal of Pharmaceutics and Biopharmaceutics* **1999,** *48* (2), 101-111; (b) Gaucher, G.; Dufresne, M.-H.; Sant, V. P.; Kang, N.; Maysinger, D.; Leroux, J.-C., "Block copolymer micelles: preparation, characterization and application in drug delivery." *Journal of Controlled Release* **2005,** *109* (1–3), 169-188; (c) Kataoka, K.; Harada, A.; Nagasaki, Y., "Block copolymer micelles for drug delivery: design,

characterization and biological significance." *Advanced Drug Delivery Reviews* **2001,** *47* (1), 113-131.

21. Schmidt-Mende, L.; Fechtenkötter, A.; Müllen, K.; Moons, E.; Friend, R. H.; MacKenzie, J. D., "Self-Organized Discotic Liquid Crystals for High-Efficiency Organic Photovoltaics." *Science* **2001,** *293* (5532), 1119-1122.

22. (a) Hirzinger, B.; Helmstedt, M.; Stejskal, J., "Light scattering studies on core–shell systems: determination of size parameters of sterically stabilized poly(methylmethacrylate) dispersions." *Polymer* **2000,** *41* (8), 2883-2891; (b) Baines, F. L.; Dionisio, S.; Billingham, N. C.; Armes, S. P., "Use of Block Copolymer Stabilizers for the Dispersion Polymerization of Styrene in Alcoholic Media." *Macromolecules* **1996,** *29* (9), 3096-3102.

23. Aniansson, E. A. G.; Wall, S. N., "Kinetics of step-wise micelle association." *The Journal of Physical Chemistry* **1974,** *78* (10), 1024-1030.

24. Lund, R.; Willner, L.; Pipich, V.; Grillo, I.; Lindner, P.; Colmenero, J.; Richter, D., "Equilibrium Chain Exchange Kinetics of Diblock Copolymer Micelles: Effect of Morphology." *Macromolecules* **2011,** *44* (15), 6145-6154.

25. Halperin, A.; Alexander, S., "Polymeric micelles: their relaxation kinetics." *Macromolecules* **1989,** *22* (5), 2403-2412.

26. (a) Dormidontova, E. E., "Micellization Kinetics in Block Copolymer Solutions: Scaling Model." *Macromolecules* **1999,** *32* (22), 7630-7644; (b) Li, Z.; Dormidontova, E. E., "Kinetics of Diblock Copolymer Micellization by Dissipative Particle Dynamics." *Macromolecules* **2010,** *43* (7), 3521-3531.

27. (a) Wang, Y.; Kausch, C. M.; Chun, M.; Quirk, R. P.; Mattice, W. L., "Exchange of Chains between Micelles of Labeled Polystyrene-block-poly(oxyethylene) As Monitored by Nonradiative Singlet Energy Transfer." *Macromolecules* **1995,** *28* (4), 904-911; (b) Underhill, R. S.; Ding, J.; Birss, V. I.; Liu, G., "Chain Exchange Kinetics of Polystyrene-block-poly(2-cinnamoylethyl methacrylate) Micelles in THF/Cyclopentane Mixtures." *Macromolecules* **1997,** *30* (26), 8298-8303.

28. Waton, G.; Michels, B.; Zana, R., "Dynamics of Block Copolymer Micelles in Aqueous Solution." *Macromolecules* **2001,** *34* (4), 907-910.

29. Lund, R.; Willner, L.; Monkenbusch, M.; Panine, P.; Narayanan, T.; Colmenero, J.; Richter, D., "Structural Observation and Kinetic Pathway in the Formation of Polymeric Micelles." *Physical Review Letters* **2009,** *102* (18), 188301.

30. Choi, S.-H.; Lodge, T. P.; Bates, F. S., "Mechanism of Molecular Exchange in Diblock Copolymer Micelles: Hypersensitivity to Core Chain Length." *Physical Review Letters* **2010,** *104* (4), 047802.

31. Lund, R.; Willner, L.; Stellbrink, J.; Lindner, P.; Richter, D., "Logarithmic Chain-Exchange Kinetics of Diblock Copolymer Micelles." *Physical Review Letters* **2006,** *96* (6), 068302.

32. Zupancich, J. A.; Bates, F. S.; Hillmyer, M. A., "Aqueous Dispersions of Poly(ethylene oxide)-b-poly(γ-methyl-ε-caprolactone) Block Copolymers." *Macromolecules* **2006,** *39* (13), 4286-4288.

33. (a) Lohmeijer, B. G. G.; Pratt, R. C.; Leibfarth, F.; Logan, J. W.; Long, D. A.; Dove, A. P.; Nederberg, F.; Choi, J.; Wade, C.; Waymouth, R. M.; Hedrick, J. L., "Guanidine and Amidine Organocatalysts for Ring-Opening Polymerization of Cyclic Esters." *Macromolecules* **2006,** *39* (25), 8574-8583; (b) Pratt, R. C.; Lohmeijer, B. G. G.; Long, D. A.; Waymouth, R. M.; Hedrick, J. L., "Triazabicyclodecene: A Simple Bifunctional Organocatalyst for Acyl Transfer and Ring-Opening Polymerization of Cyclic Esters." *Journal of the American Chemical Society* **2006,** *128* (14), 4556-4557.

34. Schuetz, P.; Greenall, M. J.; Bent, J.; Furzeland, S.; Atkins, D.; Butler, M. F.; McLeish, T. C. B.; Buzza, D. M. A., "Controlling the micellar morphology of binary PEO-PCL block copolymers in water-THF through controlled blending." *Soft Matter* **2011,** *7* (2), 749-759.

35. Taniewska-Osińska, S.; Nowicka, B.; Kacperska, A.; Bald, A., "Correlation of Viscosity Parameters and Enthalpy of Solutions of Electrolytes in Water-Organic Solvents." *Physics and Chemistry of Liquids* **1993,** *25* (2), 113-125.

36. Kline, S., "Reduction and analysis of SANS and USANS data using IGOR Pro." *Journal of Applied Crystallography* **2006,** *39* (6), 895-900.

37. Hiemenz, P. C.; Rajagopalan, R., Principles of Colloid and Surface Chemistry. 3rd ed.; CRC Press: 1997.

38. Aminabhavi, T. M.; Gopalakrishna, B., "Density, Viscosity, Refractive Index, and Speed of Sound in Aqueous Mixtures of NJV-Dimethylformamide, Dimethyl Sulfoxide, NJV-Dimethylacetamide, Acetonitrile, Ethylene Glycol,

Diethylene Glycol, 1,4-Dioxane, Tetrahydrofuran, 2-Methoxyethanol, and 2-Ethoxyethanol at 298.15 K." *J. Chem. Eng. Data* **1995,** *40*, 856-861.

39. Ratnagiri, R.; Scott, C. E., "Effect of viscosity variation with temperature on the compounding behavior of immiscible blends." *Polymer Engineering & Science* **1999,** *39* (9), 1823-1835.